Contents lists available at ScienceDirect

Neurobiology of Disease

Transcending the amyloid-beta dominance paradigm in Alzheimer's disease: An exploration of behavioural, metabolic, and gut microbiota phenotypes in 5xFAD mice

Dina Medina-Vera [a,b,c,d], Emma N. Zambrana-Infantes [e], Antonio J. López-Gambero [a,f], Julia Verheul-Campos [a], Luis J. Santín [e], Elena Baixeras [g], Juan Suarez [a,h], Francisco J. Pavon [a,d], Cristina Rosell-Valle [a,*], Fernando Rodríguez de Fonseca [a,*]

[a] Instituto de Investigación Biomédica de Málaga y Plataforma en Nanomedicina-IBIMA, Unidad de Gestión Clínica de Salud Mental, Hospital Regional Universitario de Málaga, 29010 Málaga, Spain
[b] Facultad de Ciencias, Campus de Teatinos s/n, Universidad de Málaga, 29010 Málaga, Spain
[c] Facultad de Medicina, Campus de Teatinos s/n, Universidad de Málaga, 29010 Málaga, Spain
[d] Unidad de Gestión Clínica del Corazón—CIBERCV (Enfermedades Cardiovasculares), Hospital Universitario Virgen de la Victoria, 29010 Málaga, Spain
[e] Departamento de Psicobiología y Metodología de las Ciencias del Comportamiento, Facultad de Psicología, Universidad de Málaga, 29010 Málaga, Spain
[f] University of Bordeaux, INSERM, Neurocentre Magendie, U1215, 33000 Bordeaux, France
[g] Departamento de Bioquímica y Biología Molecular, Facultad de Medicina, Universidad de Málaga, 29010 Málaga, Spain
[h] Departamento de Anatomía Humana, Medicina Legal e Historia de la Ciencia, Facultad de Medicina, Universidad de Málaga, 29010 Málaga, Spain

ARTICLE INFO

ABSTRACT

The amyloid cascade hypothesis is widely accepted as an explanation for the neuropathological changes in Alzheimer's disease (AD). However, the role of amyloid-beta (Aβ) as the sole cause of these changes is being questioned. Using the 5xFAD mouse model of AD, we investigated various factors contributing to neuropathology, including genetic load (heterozygous (HTZ) versus homozygous (HZ) condition), behavioural phenotype, neuropathology markers, metabolic physiology, and gut microbiota composition at early (5 months of age) and late (12 months of age) stages of disease onset, and considering both sexes. At 5 months of age, both HTZ and HZ mice exhibited hippocampal alterations associated with Aβ accumulation, leading to increased neuroinflammation and disrupted PI3K-Akt pathway. However, only HZ mice showed cognitive impairment in the Y-maze and Morris water maze tests, worsening with age. Dysregulation of both insulin and insulin secretion-regulating GIP peptide were observed at 5 months of age, disappearing later. Circulating levels of metabolic-regulating hormones, such as Ghrelin and resisting helped to differentiates HTZ mice from HZ mice. Differences between HTZ and HZ mice were also observed in gut microbiota composition, disrupted intestinal barrier proteins, and increased proinflammatory products in the intestine. These findings suggest that cognitive impairment in 5xFAD mice may not solely result from Aβ aggregation. Other factors, including altered PI3K-Akt signalling, disrupted insulin-linked metabolic pathways, and changes in gut microbiota, contribute to disease progression. Targeting Aβ deposition alone may not suffice. Understanding AD pathogenesis and its multiple contributing factors is vital for effective therapies.

1. Introduction

Numerous hypotheses have been proposed to explain the neuropathological origin of Alzheimer's disease (AD). However, these hypotheses face increasing challenges as they fail to fully elucidate the etiopathogenesis of this debilitating disease. The widely accepted "amyloid cascade hypothesis" suggests that the accumulation of insoluble amyloid-β (Aβ) peptides, leading to the formation of senile plaques in the central nervous system (CNS), is a key factor (Bartholomew et al., 2002; Hardy and Selkoe, 2002). Additionally, hyperphosphorylation of tau protein and the subsequent deposition of neurofibrillary tangles are implicated. Mutations in genes involved in the processing of amyloid precursor protein (APP) such as presenilin-1 (PSEN1) and − 2 (PSEN2), can generate abnormal Aβ, particularly the longer amino acid variants (i.e. Aβ 42) (Bekris et al., 2010; Hsiao et al., 1996; Tanzi and Bertram, 2005). These abnormal Aβ variants result in both toxicity and Aβ deposition (Levy-Lahad et al., 1995; Rogaev et al., 1995; Sherrington et al., 1995). These mutations are predominantly observed in inherited cases of early-onset familial AD, which account for a small percentage of all cases (J. Liu and Li, 2019). However, it is essential to acknowledge that these hypotheses should not be regarded as definitive explanations. The neuropathological origin of AD remains an open question, and other factors such as astrocyte dysfunction and neuroinflammation (Bronzuoli et al., 2019), insulin resistance (Ott et al., 1999), and alterations in the gut-brain microbiota axis (Bairamian et al., 2022) are being increasingly recognized. Continued research is necessary to unravel the complex mechanisms underlying AD and provide a comprehensive understanding of its origins.

The hippocampus is a severely affected region in individuals with Alzheimer's disease (AD). Post-mortem studies have consistently revealed the deposition of amyloid plaques in the hippocampal formation, particularly in regions such as the cornu ammonis 1 (CA1), subiculum, and entorhinal cortex (Braak and Braak, 1991; Furcila et al., 2018). However, not only the presence of Aβ deposits but also the progression of neurofibrillary tangles could predict declines in cognitive function and memory loss in AD subjects (Serrano-Pozo et al., 2011). It is well-established that the hippocampal formation is involved in memory processes (Bird et al., 2008), and is particularly vulnerable to damage caused by abnormal inflammatory responses and oxidative stress. The PI3K (phosphoinositide 3 kinases)/Akt pathway, which coordinates neuronal responses in the brain, has been shown to have significant implications for AD-related events (Long et al., 2021; O'Neill, 2013). Central insulin resistance, a common feature associated with premature aging, is observed in the early stages of neurological diseases like AD (Milstein and Ferris, 2021). Dysfunctional insulin signalling mediated by the PI3K-Akt pathway is considered a risk factor for AD development (Gabbouj et al., 2019). This pathway is involved in critical biological processes, including cell proliferation, growth, migration, and survival (Xu et al., 2020), and multiple studies suggest that Aβ oligomers inhibit the PI3K-Akt pathway, leading to neuronal death and dementia (Razani et al., 2021; Yu and Koh, 2017). Activation of the PI3K-Akt pathway can also be induced by lipopolysaccharides (LPS), which are released by bacteria primarily located in the gut (Liao et al., 2022; Sánchez-Alegría et al., 2018). LPS can cross both the intestinal barrier and blood-brain barrier (BBB), activating immune pathways in the brain and triggering neuroinflammation through the activation of reactive microglia and astrocytes(Banks, 2008; Braniste et al., 2014; Logsdon et al., 2018). In fact, the composition of the gut microbiota has gained significant interest as it can influence physiological function and behaviour, including its potential role in the development of AD (Bairamian et al., 2022; Cryan and Dinan, 2012; Kowalski and Mulak, 2019).

The 5xFAD mouse model is widely used as a preclinical model of AD that co-overexpresses human APP and human PSEN1 genes, leading to accelerated formation of amyloid plaque (Oakley et al., 2006). Cognitive impairments, particularly in hippocampus-dependent memory, have been observed in 5xFAD mice (Cho et al., 2014; Girard et al., 2014; Kimura and Ohno, 2009; Oakley et al., 2006); however, limited research has investigated the influence of genetic load on histology, physiology, and gut microbiota composition to gain a better understanding of AD development. One study reported that 5xFAD mice bred to homozygosity displayed age-dependent motor phenotypes and deficits in spatial reference memory at 2 and 5 months (Richard et al., 2015). Considering the potential interaction between genetic factors and the environment in accelerating AD progression, it is crucial to explore the role of AD-associated genes in understanding non-genetic influences on the disease's development. For instance, a recent study demonstrated the impact of alcohol consumption on cognitive impairment and amyloid deposition in 3-TG transgenic mice (Ledesma et al., 2021). To investigate whether impaired cognition in AD is solely attributable to the amyloid beta (Aβ) load in the brain or if other factors contribute to disease progression, we conducted an analysis using heterozygous (HTZ) and homozygous (HZ) transgenic 5xFAD mice at two different age groups representing early and late disease onset. By studying these mice, we aimed to determine if the combination of other factors, in addition to Aβ load, exacerbates cognitive decline and disease progression.

2. Materials and methods

2.1. Animals and ethics statement

5xFAD mice co-express and co-inherit familial Alzheimer's disease (FAD) mutant forms of human APP (the Swedish mutation: K670N, M671L; the Florida mutation: 1716 V; the London mutation: V7171) and PSI (M146L; L286V) transgenes under transcriptional control of the neuron-specific mouse Thy-1 promotor (Tg6799 line) (Oakley et al., 2006). 5xFAD lines (B6/SJL genetic background) were maintained by crossing heterozygous transgenic mice with B6/SJL F1 breeders (The Jackson Laboratory, Bar Harbor, ME, USA).

All experiments were performed in non-transgenic (no-tg), HTZ, and HZ 5xFAD transgenic female and male mice. Two life stages of mice were used: mature adult mice at 5 months of age (considered early disease onset) and middle-aged mice at 12 months of age (considered late disease onset). Mice of the same sex were housed in groups of 3–4 on a 12 h light/dark cycle (lights on at 07:00 h), with water and food provided ad libitum. Experiments were conducted between 09:00 and 15:00. Animals were housed in groups of 3–4 per cage, except during the saccharin and sucrose consumption test, for which mice were housed individually. In our study, we used a total of 14 animals per group (males and females). The distribution was done in relation to the need to conduct different types of analyses and evaluations on the same animals to obtain a more comprehensive and thorough understanding of the results. Half of the animals, specifically seven animals per group, were specifically assigned for behavioural studies and immunohistochemical techniques. The other half of the animals were used for biochemical analyses. In this case, plasma was extracted from all animals, regardless of their group assignment.

All experiments were performed in compliance with the ARRIVE guidelines (Kilkenny et al., 2010) and in accordance with the European Communities Council Directives 2010/63/EU, Regulation (EC) n° 86/609/ECC (24 November 1986) and Spanish National and Regional Guidelines for Animal Experimentation (Real Decreto 53/2013). The experimental protocols were approved by The Local Ethical Committee for Animal Research of the University of Malaga (CTS-8221, July 2016). Accordingly, every effort was made to minimize animal suffering and reduce the number of animals used.

2.2. Quantitative genotyping

Genotyping was performed by PCR analysis of ear DNA to detect the human APP gene. The primers were: common Forward: ACCCCCATGTCAGAGTTCCT, wild-type Reverse: TATACAACCTTGGGGGATGG, mutant Reverse: CGGGCCTCTTCGCTATTAC

(Invitrogen) were used to amplify the Tg transgene (APPSwFlLon, PSEN1*M146L*L286V) 6799Vas inserted on mouse chromosome 3 in 5xFAD transgenic mice. This assay can be used to distinguish between hemizygotes and homozygotes. The JAX protocol #31769 (https ://www.jax.org/Protocol?stockNumber=006554 and protocolID = 31,769) was used. PCR was performed using a Thermocycler PCR instrument (Eppendorf) under standard conditions. The PCR products were visualized on 2% agarose gel.

2.3. Behavioural assays

Mice were subjected to neurological screening, saccharin preference test (SacPT), sucrose preference test (SPT), open field (OF), elevated plus maze (EPM), Y-maze test (YMT), and Morris water maze (MWM). All tests are detailed in Supplementary Material.

2.4. Tissue and histological procedures

All the mice were sacrificed at 5 and 12 months of age. Animals were anaesthetized with 50 mg/kg pentobarbital and blood was drawn directly from the right atrium. Mice were transcranial perfused with 0.1 M phosphate-buffered saline (PBS). Faeces were then collected from the colon and immediately frozen at $-80\ °C$ for microbiota analysis. Brain samples were quickly removed and bisected down the midline; one hemibrain was used for histological and immunohistochemical procedures, and the other hemibrain was kept on dry ice and stored at $-80\ °C$ for biochemical analysis.

2.4.1. Immunohistochemistry

The hemibrains were fixed in 0.1 M PBS containing 4% paraformaldehyde (PFA) for 48 h and cryopreserved in 30% sucrose in 0.1 M PBS solution for 5 days at $4\ °C$. Cerebral hemispheres were cut 50 μm thick in the coronal plane on a microtome, and sections were performed as previously described (Castilla-Ortega et al., 2011; Medina-Vera et al., 2020; Rosell-Valle et al., 2021Medina-Vera et al., 2020). Serial sections were blocked with 5% donkey serum and 0.5% Triton X-100 in 0.1 M PBS for 45 min at room temperature (RT). To analyse amyloid-β plaques, rabbit anti-Aβ (1:500, Abcam), rabbit anti-amyloid $β_{1-40}$ ($Aβ_{40}$; 1:500, Thermo Fisher), and rabbit anti-$Aβ_{1-42}$ ($Aβ_{42}$; 1:500, Thermo Fisher) were used. For the neuroinflammatory analysis, rabbit anti-glial fibrillary acidic protein (GFAP; 1:1000; Dako Cytomation Glostrup, Denmark) and rabbit anti-Iba1 (1:500, Abcam) were used. Primary antibodies were incubated overnight at RT. After rinsing, the sections were incubated with biotinylated goat anti-rabbit secondary antibody (1:800, GE Healthcare) for 2 h at RT. All the antibodies were diluted in PBS, 0.5% Triton X-100, and 2.5% donkey serum. The peroxidase-conjugated extra-avidin method and diaminobenzidine as the chromogen were used to visualize the reaction product.

The numbers of labelled Aβ plaques were manually counted in the hippocampus (CA1, CA3, and dentate gyrus (DG)). For the quantification of GFAP and Iba1 staining, we employed densitometry analysis using ImageJ software (Analyse > Set Measurements: Area and Integrated Density; Analyse > Measure). Images were acquired using a DP70 digital camera (Olympus Iberia, S.A.U.) connected to an Olympus BX41 microscope. The ImageJ software was used for immunostaining quantification (Schneider et al., 2012). The images were binarized to 16-bit black and a fixed intensity threshold was applied for each immunostaining. Eight mice per group and three sections per mouse were used at three different hippocampal levels.

2.4.2. Western blot analysis

Frozen hemibrain samples (17 mg per sample) were dissected and homogenized in 1 mL of cold RIPA lysis buffer (50 mM Tris-HCl pH 7.4, 150 mM NaCl, 0.5% NaDOC, 1 mM EDTA, 1% Triton, 0.1% SDS, 1 mM Na3VO4, 1 mM NaF) supplemented with a protease cocktail (Hoffmann-La Roche). The suspension was incubated for 2 h at $4\ °C$, followed by centrifugation at 12,000 rpm for 15 min at $4\ °C$. The supernatant was transferred to a new clean centrifuge tube and the Bradford colorimetric method was used to determine the total protein concentration. Protein extracts were diluted 1:1 in loading buffer (DTT $2\times$) and heated for 5 min at $99\ °C$ before being subjected to electrophoresis.

Protein expression, including IRS1, PI3K p85, Akt, GSK-3β, mTOR, and Tau, was analysed by western blotting. Tissue protein (10-15 μg) was subjected to electrophoresis on 4–12% Criterion XT Precast Bis-Tris gels (Bio-Rad, Hercules, CA, USA) for 30 min at 80 V and 2 h at 150 V. Proteins were transferred onto a 0.2 μm nitrocellulose membrane (Bio-Rad, Hercules, CA, USA) for 1 h at 80 V using wet transfer equipment. The membrane was washed twice for 5 min in TBST (10 mM Tris–HCl, 150 mM NaCl, 0.1% Tween 20, pH 7.6) and blocked with 5% BSA-TBST for 1 h at RT on a shaker platform. Subsequently, the membrane was incubated with the respective primary antibodies overnight at $4\ °C$ and diluted in 2% BSA-TBST (detailed in Supplementary Material Table S1). The following day, the membrane was washed thrice for 5 min with TBST. An appropriate HRP peroxidase-conjugated rabbit/mouse secondary antibody (Promega, Madison, WI, EE.UU.) was diluted 1:10000 in 2% BSA-TST and incubated with the membrane for 1 h of shaking at RT. Finally, the membrane was washed as described above and exposed to chemiluminescent reagent using the Western Blotting Luminol Reagent kit (Santa Cruz Biotechnology, Santa Cruz, CA, USA) for 1 min. Membrane-bound proteins were visualized by chemiluminescence using a Chemi-Doc TM MP Imaging System (Bio-Rad, Barcelona, Spain). After detecting phosphorylated proteins, specific antibodies were removed from the membrane by incubating with stripping buffer (2% SDS, 62.5 mM Tris HCl (pH 6.8), 0.8% β-mercaptoethanol) for 30 min at $50\ °C$. Membranes were thoroughly cleaned in ultrapure water before being pre-incubated with the corresponding total antibody. Bands were quantified by densitometry analysis using the ImageJ software (Schneider et al., 2012). Normalization was performed using a reference protein from the same membrane, γ-adaptin protein. The results were presented as the ratio of total protein expression to γ-Adaptin and the ratio of phosphorylated protein expression to total protein expression (Bass et al., 2017).

2.5. Bio-Plex multiplex assay

Plasma levels of insulin, gastric inhibitory polypeptide (GIP), glucagon-like peptide-1 (GLP-1), leptin, ghrelin, glucagon, resistin, and plasminogen activator inhibitor-1 (PAI-1) were measured using a multiplex immunoassay system with a commercial kit (Bio-Plex Pro™ mouse diabetes 8-plex immunoassay, Bio-Rad, Hercules, CA, USA, cat. number: #171F7001M). Plates were run on a Bio-Plex MAGPIX™ Multiplex Reader with Bio-Plex Manager™ MP Software (Luminex, Austin, TX, USA). Hormone concentrations were expressed in pg/mL, and detection limits were 68.29 (insulin), 4.31 (GIP), 0.59 (GLP-1), 5.07 (leptin), 0.64 (ghrelin), 0.50 (glucagon), 184.89 (resistin) and 2.98 (PAI-1) pg/mL.

2.6. Aβ soluble quantification: ELISA

The hippocampus was homogenized in buffer (5 M guanidine-HCl/ 50 mM Tris, pH 8.0), and protease inhibitor cocktail (Roche Molecular Systems, Pleasanton, CA, USA). Homogenate Centrifuge at $16,000\ \times g$ for 20 min at $4\ °C$, and the supernatant was saved as the soluble fraction for Aβ quantifications. The Aβ42 human enzyme-linked immunosorbent assay (ELISA) kit (Catalog # KMB3441, Invitrogen™ Mouse Aβ42 ELISA Kit) was used to quantify Aβ42 levels according to the manufacturer's instructions.

2.7. RNA isolation and real-time q-PCR

Total RNA was extracted from tissue sections of the small intestine (50–80 mg) using the TRIzol ® method, according to the manufacturer's

instructions (Invitrogen, Carlsbad, CA, USA). RNA samples were isolated using an RNA easy minelute cleanup-kit including digestion with DNase I column (Qiagen) and quantified using a spectrophotometer to ensure A260/280 ratios of 1.8–2.0. Reverse transcription was performed from 1 μg of RNA using the Transcriptor Reverse Transcriptase kit (Transcriptor RT, Roche Applied Science, Mannheim, Germany) and specific sets of primer probes (Cldn3: Mm00515499_s1, amplicon length:60; Ocln: Mm00500910_m1, amplicon length:83; Tlr4: Mm00445273_m1; amplicon length:87) from TaqMan® Gene Expression Assays (TaqMan, Thermo Fisher Scientific, Waltham, MA, USA). Real-time qPCR reactions were carried out using a CFX96TM Real-Time PCR Detection System (Bio-Rad, Hercules, CA, USA) and the FAM dye labelled format for the TaqMan® Gene Expression Assays (Thermo Fisher Scientific). Melting curve analysis was performed to ensure that only a single product was amplified. We normalized the values obtained from the small intestine samples in relation to GAPDH levels (Mm99999915_g1, amplicon length:107; Thermo Fisher Scientific).

2.8. Gut microbiota analysis

Gut microbiota analysis was performed as previously described (Segovia-Rodríguez et al., 2022). Colon faeces samples at 5 and 12 months of age (180–200 mg) were used for DNA extraction. A QIAamp® DNA Stool Mini Kit (Qiagen France S.A.S.) was used according to the manufacturer's instructions. DNA concentration and purity were determined by absorbance at 260 nm (A260) and the A260/A280 ratio, respectively, using a NanoDrop spectrophotometer (NanoDrop TM One Spectrophotometer, Thermo Fisher Scientific Inc., Spain). DNA samples were sent to StarSEQ® GmbH (Mainz, Germany) for analysis of the V3–V4 hypervariable regions of the bacterial 16 S rRNA gene, amplified from the isolated DNA using the primer combination 515F–909 R. The Illumina MiSeq System was used to sequence DNA products of this PCR amplification and 16 S metagenomics analysis was performed using QIIME 2 (Bolyen et al., 2019) version 2023.5 in a conda environment which is based on the Ubuntu Linux operating system. The taxonomy database used was Silva 138.1 version (Quast et al., 2013), and the RESCRIPt plugin was employed for its curation and preparation. Phylum analysis focused on both the *Bacteroidetes* and *Firmicutes* phyla. Taxonomic compositions were compared at family level in terms of relative abundance using QIIME 2.

2.9. Statistical analyses

For data obtained from neurological screening, the nonparametric Kruskal-Wallis test were used. Behavioural tests, western blotting analysis, and immunostaining quantification were evaluated by a two-way analysis of variance (ANOVA) with the factors "age" and "genotype". Subsequently, a Tukey post-hoc test was conducted for multiple comparisons. In the MWM, thigmotaxis behaviour and learning parameters were analysed separately by one-way ANOVA, repeated measures two-way ANOVA ("genotype" x "trial session" [day]), and two-way ANOVA ("genotype" x "training day"). For comparisons between two groups, we also employed Student's *t*-test. To assess the potential influence of hyperdynamic locomotion on cognitive deterioration in the Y-maze test, we calculated Pearson's correlation coefficient (Miedel et al., 2017). Statistical significance was set at $P \leq 0.05$.

For microbiota analysis, sequencing data was processed and analysed using specific software and packages. The paired-end sequences of each sample were exported in FASTQ format. The quality of the sequences was first assessed using the FastQC software. For the quantitative analysis of the relative abundance of the microbiota in the samples, R 4.1.2 was used in the Rstudio working environment, version 2023.03.1. The analysis utilized the "stats", "xlsx", "car," "dplyr," and "readr" packages, along with the Bioconductor "bio format" package. A paired-end demultiplexed sequencing protocol was used to import the sequences, and the dada2 denoise-paired command (Callahan et al.,

2016) was employed for used for quality filtering, denoising, and merging of paired-end reads. Core metrics were obtained to assess alpha and beta diversities. Alpha diversity measures the species richness within each community, while beta diversity examines the differences in composition, specifically the abundance of different taxa, among different samples. Alpha rarefaction analysis was performed at a depth of 25,000 per sample. The sequences were grouped into operational taxonomic units (OTUs) using a 97% similarity threshold. Taxonomic assignment was carried out using an own trained classifier using the q2-feature-classifier plugin (Bokulich et al., 2018). Statistical inference was performed using the Kruskal–Wallis test and Mann-Whitney U for each OTUs, allowing for comparisons and identification of significant differences between groups. The entire generated information, along with the used scripts, has been hosted on the following link: github.com/VerheulJ/5XFAD.

To identify underlying patterns and reduce the dimensionality of the data, clustering and ordination methods were employed. Specifically, Principal Component Analysis (PCA) was applied to the behavioural variables, neuroinflammation, PI3K/Akt pathway, insulin-linked metabolic pathway, and *Firmicutes/Bacteroidetes* ratio. PCA was followed by varimax orthogonal rotation to ensure that the extracted factors were independent of each other. Factors with eigenvalues >1 were selected, indicating their significant contribution in explaining the data variance. The factor loading, which represents the contribution of each variable to a factor, was considered significant if it exceeded an absolute value of 0.5.

To address the potential issue of Type-1 error arising from multiple outcome measures, power analysis and sample size estimation were performed before the initiation of the study. Effect sizes were estimated based on previous literature to ensure adequate statistical power for the multitude of outcome measures. Additionally, adjustments for multiple comparisons were considered in our statistical analyses to enhance the reliability of the findings.

The data were presented as mean ± standard error of the mean (SEM). Statistical analyses were conducted using GraphPad Prism version 9 (GraphPad Software, Inc., La Jolla, CA, USA) for general analyses, while R software was used specifically for microbiota analysis.

3. Results

3.1. HZ 5xFAD mice showed severe neurological deficits

A battery of neurological procedures was conducted to evaluate the somatosensory and sensorimotor reflexes of HTZ and HZ mice. At 5 months of age, no significant differences were observed between the HTZ and HZ mice, indicating similar neurological function. However, at 12 months of age, HZ mice displayed greater neurological deficits compared to the age-matched no-tg mice. The deficits were observed in various reflexes, including head shaking ($P < 0.05$), corneal reflexes ($P < 0.05$), vibrissae ($P < 0.05$), auditory reflexes ($P < 0.05$), righting reflexes ($P < 0.05$), and extension reflexes ($P < 0.0001$). In contrast, HTZ mice showed preserved neurological function with age, indicating a lack of significant impairment in these reflexes. Table 1 provides detailed information on the specific reflexes assessed and the corresponding statistical results.

3.2. HTZ and HZ 5xFAD mice showed a different taste profile with a preference for a palatable sweet solution

The saccharin (SacPT) and sucrose (SPT) preference tests were conducted to assess anhedonia, a reduced ability to experience pleasure, in the mice. The SPT is also indicative of motivation for caloric foods. A two-way ANOVA was performed to analyse the effects of genotype and age on the SacPT results. The results showed significant effects of genotype ($P < 0.001$) and age ($P < 0.01$) on saccharin intake. Specifically, HZ mice at 12 months of age exhibited significantly higher saccharin

Table 1
Neurological screening at non-transgenic (No-tg), heterozygous (HTZ) and homozygous (HZ) transgenic 5xFAD mice.

Neurological tests		5 months of age			12 months of age		
		No-Tg	HTZ	HZ	No-Tg	HTZ	HZ
Vibrissae	Absent deficit (%)	100.00	100.00	100.00	100.00	57.14	50.00
	Weak deficit (%)	–	–	–	–	42.86	16.67
	Strong deficit (%)	–	–	–	–	0.00	**33.33***
Head shaking	Absent deficit (%)	100.00	100.00	100.00	100.00	100.00	66.67
	Weak deficit (%)	–	–	–	–	–	**33.33***
	Strong deficit (%)	–	–	–	–	–	–
Somesthesis	Absent deficit (%)	80.00	80.00	28.57	75.00	71.43	58.33
	Weak deficit (%)	20.00	20.00	14.29	7.69	–	8.33
	Strongdeficit (%)	–	–	57.14	15.38	28.57	33.33
Olfaction test	Absent deficit (%)	100.00	100.00	100.00	50.00	57.14	16.67
	Weak deficit (%)	–	–	–	16.67	28.57	58.33
	Strong deficit (%)	–	–	–	33.33	14.29	25.00
Corneal reflex	Absent deficit (%)	80.00	80.00	71.43	66.67	71.43	25.00
	Weak deficit (%)	20.00	20.00	14.29	30.77	28.57	**75.00***
	Strong deficit (%)	–	–	14.29	–	–	–
Auditory reflex	Absent deficit (%)	100.00	100.00	71,43	83.33	42.86	16.67
	Weak deficit (%)	–	–	28,57	–	28.57	16.67
	Strong deficit (%)	–	–	–	16.67	28.57	**66.67***
Righting reflex	Absent deficit (%)	100.00	100.00	85.71	100.00	100.00	58.33
	Weak deficit (%)	–	–	–	–	–	33.33
	Strong deficit (%)	–	–	14.29	–	–	**8.33****
Inclined plane test	Absent deficit (%)	100.00	100.00	85.71	100.00	100.00	100 0.00
	Weak deficit (%)	–	–	–	–	–	–
	Strong deficit (%)	–	–	14.29	–	–	–
Extension reflex	Absent deficit (%)	100.00	100.00	71.43	100.00	100.00	33.33
	Weak deficit (%)	–	–	–	–	–	41.67
	Strong deficit (%)	–	–	28.57	–	–	**25.00****

Data are expressed as the percentage of animals.
Differences between genotype (Dunn's test): *$P < 0.05$; **$P < 0.01$.
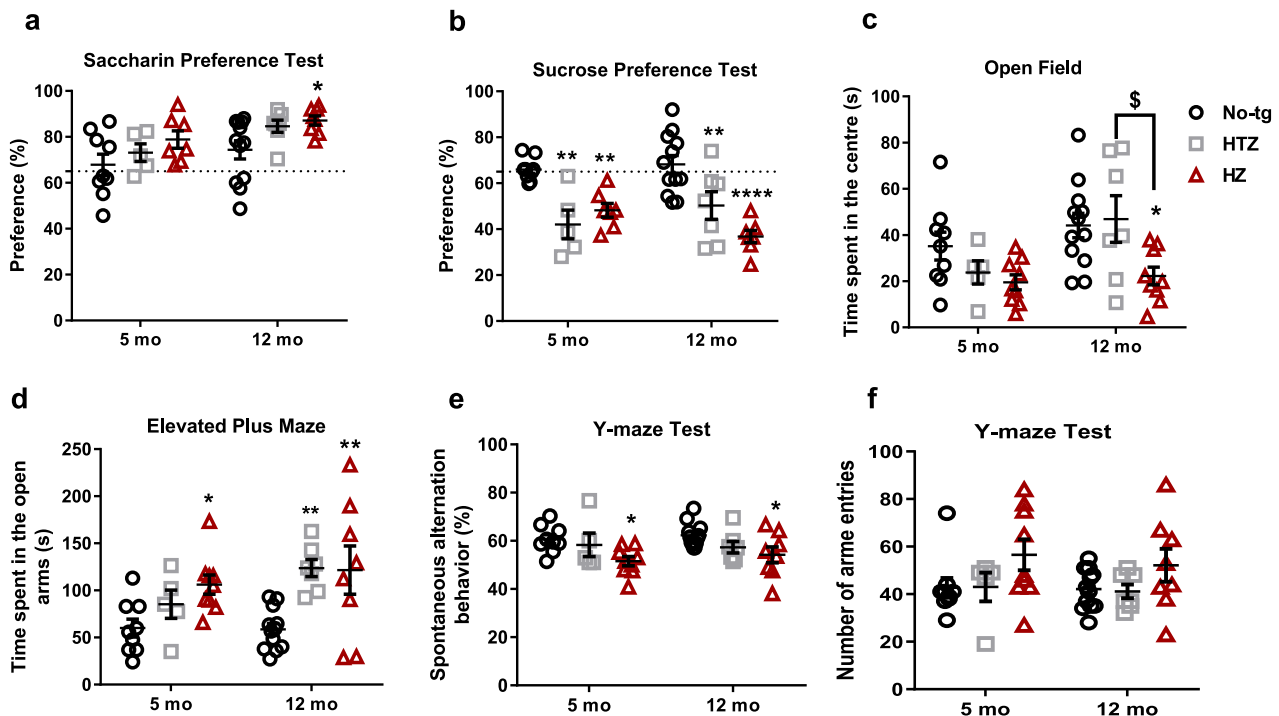

Fig. 1. Behavioural tests in heterozygous and homozygous 5xFAD mice. Saccharin preference test (a) and Sucrose preference test (b) at 5 months and 12 months of age. Dashed lines represent the criterion for anhedonia ≤65%. The time spent in the centre of the open field (c) and the time spent in the open arms (d) at 5 months and 12 months of age. Percentage of spontaneous alternation behaviour (e) and the number of entries in arms (f) in the Y-maze test at 2 points. All data represent the mean ± SEM. ($n = 7$–9). Tukey's Test: difference transgenic (HTZ and HZ) vs non-transgenic (No-tg) mice. (*) $P < 0.05$; (**) $P < 0.01$, (****) $P < 0.0001$; difference between HTZ and HZ condition: ($) $P < 0.05$.

intake compared to age-matched non-transgenic mice (Tukey's test: $P <$ 0.05, Fig. 1a). For SPT, a genotype × age interaction was observed (two-way ANOVA: $P < 0.05$). *Post-hoc* analysis revealed that both HTZ and HZ mice, starting from 5 months of age and continuing with age, exhibited significantly decreased sucrose intake compared to no-tg mice (Tukey's test: $P < 0.05$, Fig. 1b). This indicates that the transgenic 5xFAD mice had a preference for sucrose below the anhedonic threshold of 65% (one-simple test: $P < 0.05$). The weights of the animals during both tests are provided in Supplementary Material S1a and S1b. Despite the lower preference of rodent for saccharine when compared with sucrose (Hammer, 1967), the discrepancy observed in sucrose versus saccharine preference might indicate complex alternations in the processing of taste/reinforcement/post-ingestion effects in the 5xFAD model caused, among other factors, by glial activation and metabolic dysfunctions in the hypothalamus (López-Gambero et al., 2021). For more details, see the discussion section.

3.3. HTZ and HZ 5xFAD mice showed an abnormal emotional response in OF and EPM

To evaluate the emotional status and anxiety-like behaviours, the OF and EPM were conducted. Two-way ANOVA analysis revealed significant effects of genotype ($P < 0.01$) and age ($P < 0.05$) on the time spent in the centre of the OF (Fig. 1c). At 12 months of age, HZ mice exhibited reduced time spent in the centre of the OF compared to age-matched HTZ and no-tg mice (Tukey's test: $P < 0.05$). However, no significant differences in locomotion were observed between the genotypes (Supplementary Material S1c).

Surprisingly, in EPM, 5-month-old HZ mice showed significantly increased time spent in the open arms compared to both HTZ and no-tg mice (one-way ANOVA: $P < 0.01$). This difference was maintained with age compared to no-tg mice (Tukey's test: $P < 0.05$, Fig. 1d). In contrast, HTZ mice exhibited increased time in the open arms at 12 months of age compared to no-tg mice (Tukey's test: $P < 0.05$, Fig. 1d). Similar to the OF test, there were no significant differences in locomotion between the genotypes (Supplementary Material S1d). These contradictory results may be attributed to the sensory deficits or abnormal sensation of vibration in the HZ mice shown above, preventing them from assessing the risks of the exposed arms in the EPM (Flanigan et al., 2014). For more details, see the discussion section."

3.4. HZ 5xFAD mice showed impaired spatial working memory

Y-maze test was conducted to assess spatial working memory, specifically spontaneous alternation behaviou(SAB). HZ group exhibited impaired working memory starting from 5 months of age (two-way ANOVA: genotype effect: $P < 0.01$) compared to non-transgenic littermates. HZ mice displayed a significant reduction in the percentage of SAB (Tukey's test: $P < 0.05$, Fig. 1e). This significant difference was maintained with age compared to no-tg mice (Tukey's test: $P < 0.05$, Fig. 1e). No significant differences were observed between genotypes in terms of the number of arm entries and locomotion (Fig. 1f and Supplementary Material S1e). Furthermore, there was no correlation between SAB and the number of arm entries and locomotion (Pearson's comparisons: $P > 0.05$, Supplementary Material S1f), suggesting that the observed cognitive impairment specifically in the HZ group was not influenced by locomotor or exploratory activities.

3.5. HZ 5xFAD mice showed impaired cognitive flexibility in the Morris water maze

Spatial reference learning and memory were assessed using MWM. In the habituation training, no significant differences were found between genotypes in path length and swimming speed at either age (one-way ANOVA: $P > 0.05$, Supplementary Material S2a-d).

During visual learning, surprising results were found. At 5 months of

age, HTZ mice showed a longer escape latency compared to age-matched HZ and no-tg mice on the first day of training (two-way ANOVA: genotype effect: $P < 0.0001$; trial session effect: $P < 0.05$; Tukey's test: $P < 0.05$ Supplementary Material S2e). However, by the second day of training, HTZ mice learned the platform location as efficiently as no-tg mice. Additionally, 5-month-old HTZ mice showed a higher cumulative distance to reach the visible platform on the first day of training compared to the no-tg group (two-way ANOVA: genotype x trial session interaction: $P < 0.05$, see Supplementary Material 2f). No significant differences were observed between genotypes in path length in the peripheral zone (two-way ANOVA: $P > 0.05$, see Supplementary Material S2g). In contrast, 12-month-old HZ mice exhibited longer escape latency (two-way ANOVA: $P < 0.0001$; trial session effect: $P < 0.0001$; Tukey's test: $P < 0.05$, Supplementary Material S2h) and cumulative distance (two-way ANOVA: genotype effect: $P < 0.01$; trial session effect: $P < 0.05$; Tukey's test: $P < 0.05$, Supplementary Material S2i) compared to no-tg mice. Furthermore, swimming strategies differed according to the genotype and age, with 12-month-old HZ mice displaying a 'wall-hugging' or thigmotaxis (time spent in the peripheral zone) behaviour during visual learning, while HTZ and no-tg mice showed a direct search pattern to reach the platform (two-way ANOVA: *genotype* effect: $P < 0.0001$; *day* effect: $P < 0.0001$; Tukey's test: $P < 0.05$, Supplementary Material S2j). Notably, a positive correlation was found between time spent in the peripheral zone and escape latency during navigation in all mice ($r^2 = 0.76$, $P < 0.05$), indicating that spending more time in the peripheral zone was associated with longer escape latency (Supplementary Material S2k).

During the acquisition of spatial learning, all animals were able to successfully learn the position of the hidden escape platform in target quadrant 1 (Q1) at both 5 months and 12 months of age, although 5-month-old HTZ mice showed a worse learning curve (two-way ANOVA: genotype effect: $P < 0.0001$, Tukey's test: $P < 0.05$, Fig. 2a) and cumulative distance to reach the hidden platform (two-way ANOVA: genotype effect: $P < 0.0001$, Tukey's test: $P < 0.05$, Supplementary Material S2l) compared to no-tg mice. At 12 months of age, HTZ mice were efficient in reaching the goal; thus, they did not show noticeable memory impairment (Fig. 2b). In the HZ condition, 12-month-old HZ mice showed increased escape latency, cumulative distance and thigmotaxis behaviour compared to no-tg mice (two-way ANOVA: escape latency: genotype effect: $P < 0.0001$; trial session effect: $P < 0.01$, Fig. 2b; cumulative distance: genotype effect: $P < 0.0001$; trial session effect: $P < 0.001$; Turkey's test: $P < 0.05$, Supplementary Material S2m; thigmotaxis: genotype effect: $P < 0.001$; training day effect: $P < 0.05$; Tukey's test: $P \leq 0.05$, Supplementary Material S2n).

Interestingly, no significant differences were found between the HTZ and HZ groups and the no-tg group in the first memory retention test at any age (Fig. 2c and d). All mice spent more time in the target Q1 (two-way ANOVA: 5 months: quadrant effect: $P < 0.0001$; 12 months: quadrant effect: $P < 0.0001$). Supplementary Material S2o shows the path travelled in memory retention Test 1. In reversal spatial learning, 5-month-old HZ mice took significantly longer to reach the location of the new platform in Q3 (one-way ANOVA: $P < 0.05$; Fig. 2e), and this difference was more noticeable at 12 months of age (one-way ANOVA: $P < 0.05$; Fig. 2f). The second memory retention test was performed 24 h after reversal training. The 5-month-old HZ mice continued to remember the location of the previous platform in Q1 for a longer duration compared to the non-tg mice (two-way ANOVA: 5 months: quadrant effect: $P < 0.01$; 12 months: genotype effect: $P < 0.01$; quadrant effect: $P < 0.0001$; Tukey's test: $P < 0.05$, Fig. 2g and h). Supplementary Material S2p shows the path travelled in memory retention test 2. Memory extinction deficits were assessed, and at 5 months of age, all genotypes showed memory extinction by spending less time in Q1 after 72 h (two-way ANOVA: time effect: $P < 0.01$; Fig. 2i). Nevertheless, at 12 months, significant memory extinction impairment was observed in HZ mice, as they showed a higher preference for the first goal and perseverative navigation even after 72 h, indicating a lack of cognitive
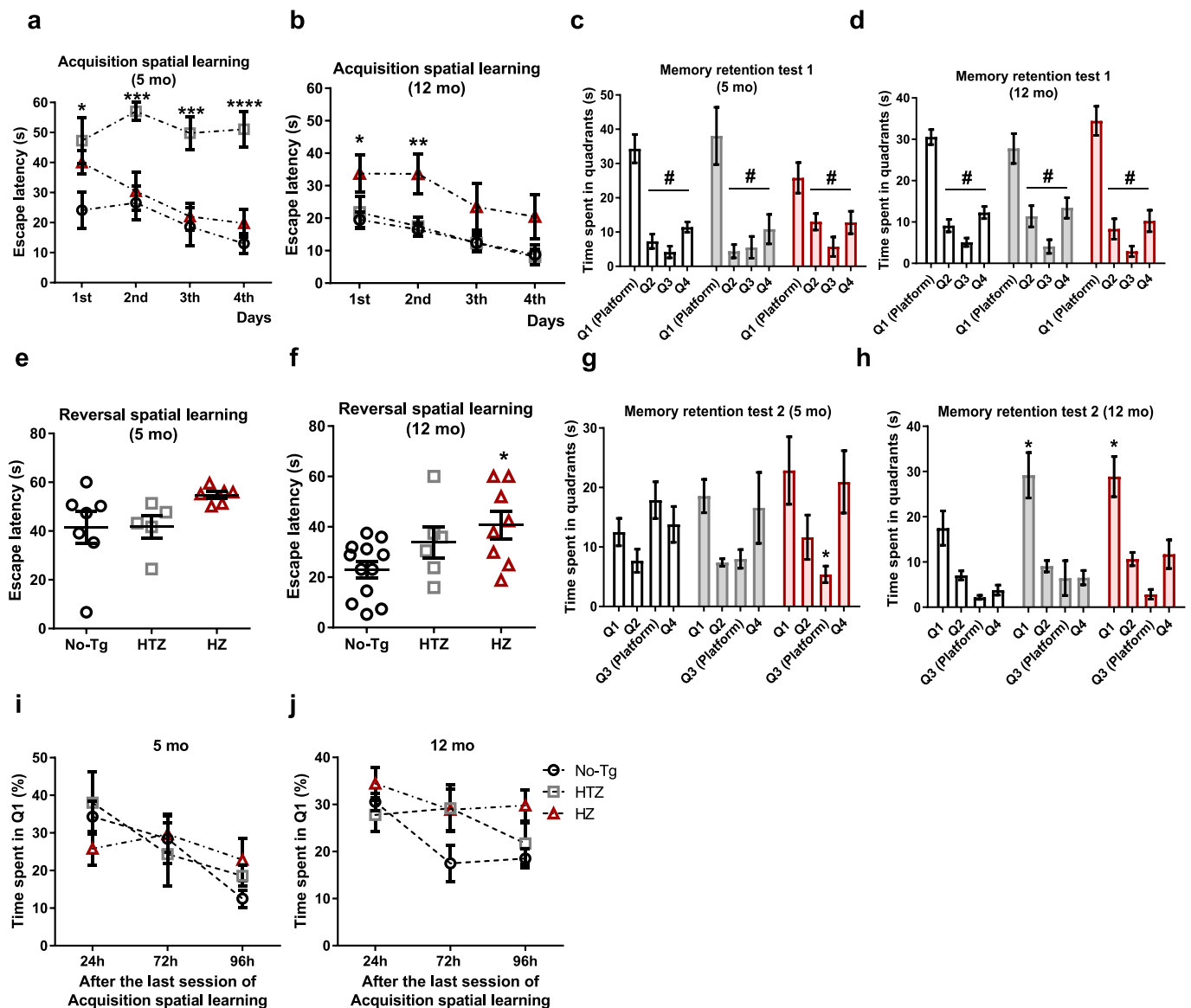
Fig. 2. Spatial learning in heterozygous and homozygous 5xFAD mice. Escape latency in the acquisition spatial learning at 5 months (a) and at 12 months of age (b). Mice received six trials over four days with 30-min intervals and the hidden platform was consistently located in Quadrant 1. Time spent in the quadrants in the memory retention test at 5 months (c) and 12 months of age (d) was conducted after 24 h of the acquisition spatial learning. Escape latency in the reversal spatial learning at 5 months (e) and 12 months of age (f). Mice received six trials over one day with 30-min intervals and the hidden platform was consistently located in Quadrant 3. Time spent in the quadrants in the memory retention test at 5 months (g) and 12 months of age (h) was conducted after 24 h of the reversal spatial learning. Time spent in the quadrant 1 (Q1) after the last session of the acquisition spatial learning at 5 months (i) and 12 months of age (j). All data represent the mean ± SEM, n = 7–9. Tukey's Test: difference between transgenic vs non-transgenic mice: (*) $P < 0.05$, (**) $P < 0.01$, (***) $P < 0.001$, (****) $P < 0.0001$; difference between quadrant 1 (Q1): (#) $P < 0.05$.

flexibility in this age range for developing new spatial learning (two-way ANOVA: genotype effect: $P < 0.01$, time effect: $P < 0.05$; Tukey's test: $P < 0.05$, Fig. 2j).

3.6. Hippocampal dysfunction in HTZ and HZ 5xFAD mice

To determine whether the genetic loading led to a differential pattern of Aβ deposition in HTZ and HZ mice, we quantified Aβ40, Aβ42, and total Aβ in the DG, CA1, and CA3 regions of the hippocampus. As predicted, Aβ accumulation was dramatically increased throughout the hippocampus in both HTZ and HZ mice at 5 months of age. The deposition pattern of Aβ40 was similar in HTZ and HZ mice and did not vary with age (two-way ANOVA: 'genotype': $P < 0.0001$, 'hippocampus area': $P < 0.05$, Fig. 3a and b). In contrast, Aβ42 deposition in the DG and CA1 regions increased with age specifically in HZ mice (two-way

ANOVA: 'genotype': $P < 0.0001$, Tukey's test: $P < 0.05$, Fig. 3c and d), while it remained relatively constant in HTZ mice. HTZ and HZ mice had comparable levels of total Aβ at 5 and 12 months of age (two-way ANOVA: 'genotype': $P < 0.0001$, 'hippocampus area': $P < 0.0001$, Fig. 3e and f). We further enhanced our investigation by complementing the immunohistochemistry quantification with ELISA measurements of soluble Aβ42 in the hippocampus. In Fig. 3g, the authors provide supporting evidence for the immunohistochemistry results, showing a marked increase in soluble Aβ42 levels in both HTZ and HZ groups compared to the No-Tg group of the same age (two-way ANOVA: 'genotype': $P < 0.0001$, Tukey's test: $P < 0.05$, Fig. 3g). Additionally, the HZ group exhibited significantly higher Aβ42 levels than the HTZ group at both age groups (Tukey's test: $P < 0.001$). When considering age as the sole factor, the HZ group showed a significant increase in Aβ42 at 12 months of age (Tukey's test: $P < 0.0001$). These results strongly align
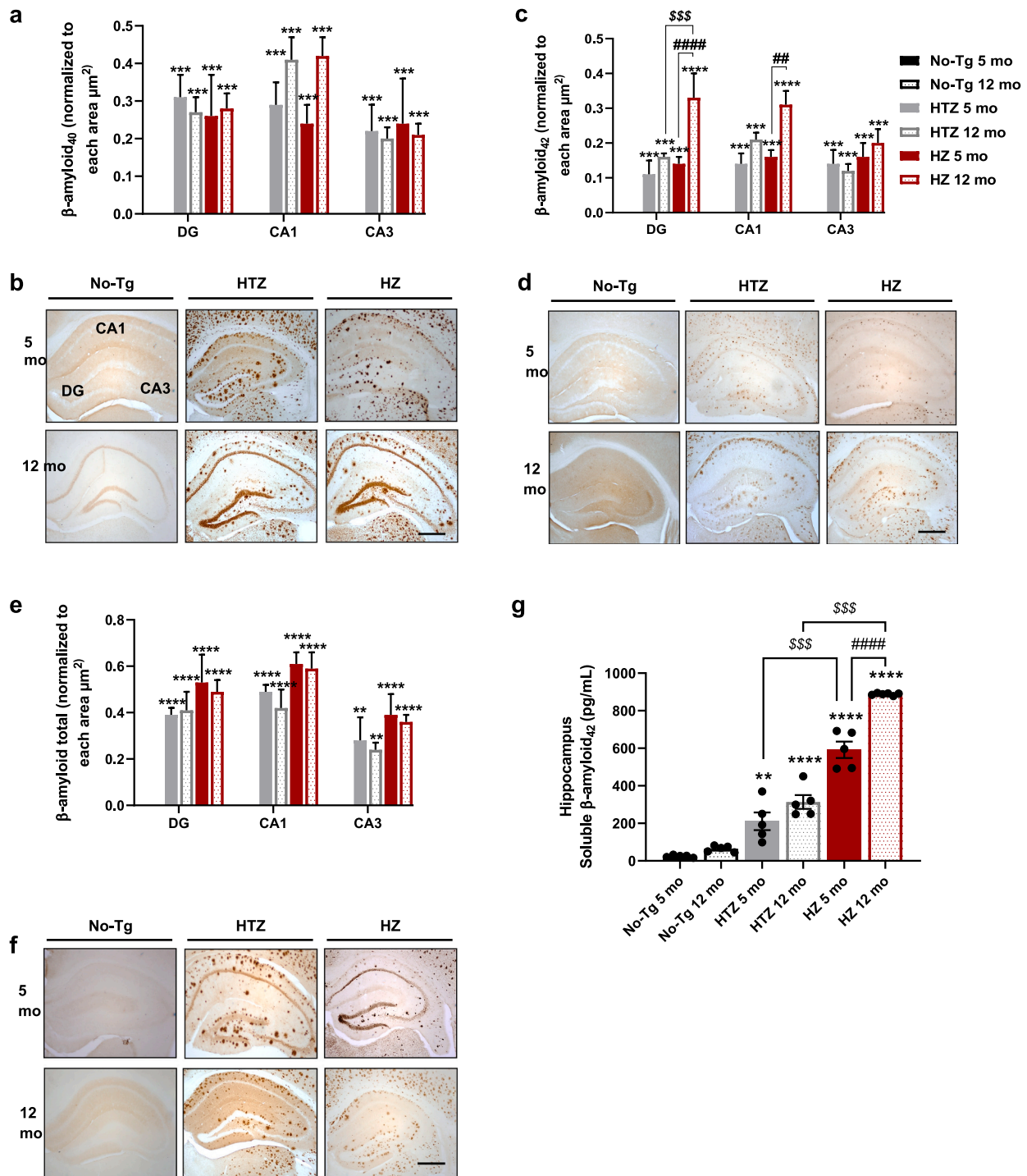
Fig. 3. Amyloid-β accumulation in the hippocampus of heterozygous and homozygous 5xFAD mice. Histograms represent the immunohistochemistry quantification of β-amyloid 1–40 (Aβ40) (a), β-amyloid 1–42 (Aβ42) (c), and total β-amyloid (e) in the hippocampus of three genotypes at 5 months and 12 months of age. Images correspond to representative immunostaining of Aβ40 (b), Aβ42 (d), and total of Aβ (f). The measurements in the no-tg group were obtained and consistently recorded as zero. Scale bar: 100 μm. (g) Soluble cerebral β-amyloid 1–42 levels from hippocampus homogenates were analysed by Aβ42 human ELISA. Aβ concentrations are expressed in picograms per millilitres (pg/mL). Histograms represent the mean ± SEM. (n = 7–9). Tukey's Test: difference between transgenic vs non-transgenic mice of the same age: (**) $P < 0.01$, (***) $P < 0.001$ and (****) $P < 0.0001$; difference between HTZ and HZ condition: ($\$\$\$$) $P < 0.001$; difference between aged group: (##) $P < 0.01$, (####) $P < 0.0001$.

with the findings from the immunohistochemistry quantification.

Regarding neuroinflammatory responses, 5-month-old HZ mice exhibited a more pronounced increase in GFAP densitometry in the DG, CA1, and CA3 regions compared to age-matched no-tg and HTZ mice (two-way ANOVA: 'genotype': $P < 0.0001$, Tukey's test: $P < 0.05$ Fig. 4a and b). However, no age-related increase was observed in either HTZ or

HZ mice. Furthermore, both HTZ and HZ mice showed elevated in Iba1 densitometry in the DG, CA1, and CA3 regions starting from 5 months of age, compared to no-tg mice (two-way ANOVA: 'genotype': $P < 0.0001$, Tukey's test: $P < 0.05$, Fig. 4c and d). Again, no age-related increase in Iba1 was observed.

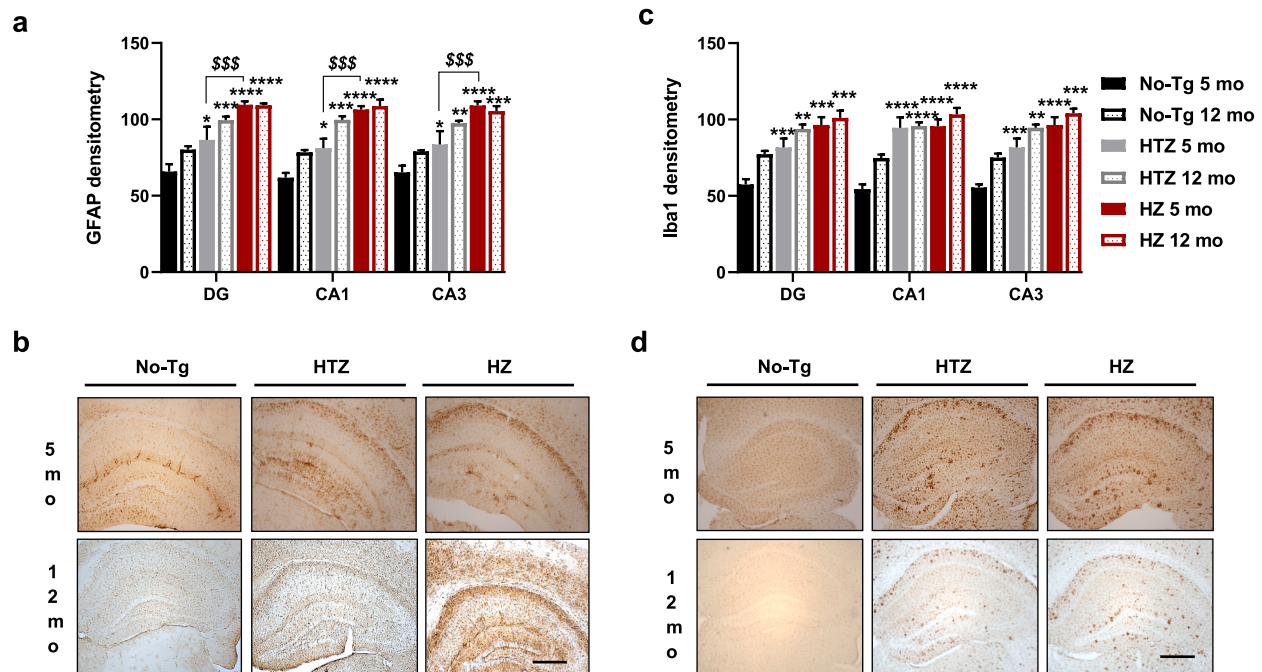On the other hand, we examined the activation and inhibition of the

Fig. 4. GFAP and Iba1 densitometry in the hippocampus at 5 months and 12 months of age. Histograms represent the immunohistochemistry quantification of GFAP (a) and Iba1 (c) in the hippocampus of three genotypes at 5 months and 12 months of age. Images correspond to representative immunostaining of GFAP (b) and Iba1 (d). Scale bar: 100 μm. Histograms represent the mean ± SEM. (n = 7–9). Tukey's Test: difference between transgenic vs non-transgenic mice of the same age: (**) $P < 0.01$, (***) $P < 0.001$ and (****) $P < 0.0001$; difference between HTZ and HZ condition: ($$$) $P < 0.001$.

IRS1-PI3K-Akt pathway, which plays a crucial role in healthy aging and is primarily activated by insulin. Western blot analysis of the insulin-PI3K-Akt signalling pathway was conducted in the hippocampus of 5xFAD transgenic mice at 5 months and 12 months of age (Fig. 5 and Supplementary Material S3 and S4). Initially, we assessed the phosphorylation of IRS1, the initial component of the Akt pathway. Serine 612 phosphorylation, associated with IRS1 signalling inactivation towards PI3K, was found to be enhanced in the HZ group at 12 months compared to 5 months of age, indicating IRS1 inhibition (two-way ANOVA: interaction: $P < 0.01$; Fig. 5a). This effect was specific to 12-month-old HZ mice and significantly higher compared to the younger group (Tukey's test: $P < 0.01$, Fig. 5a), suggesting hypoactivity of the insulin receptor due to insufficient insulin activation. Next, we examined the active phosphorylation state of PI3K (p-PI3K) and Akt (p-Akt). The activating phosphorylation of the p85 PI3k at tyrosine 607 exhibited a significant decrease in both the HTZ and HZ groups at 5 months of age, which was restored in both groups at 12 months of age (two-way ANOVA: interaction: $P < 0.01$; Fig. 5b). However, the total levels of PI3K protein remained unchanged (Fig. 5b). Similarly, the activating phosphorylation of Akt at Serine 473 showed a significant decrease in the HZ groups at 5 months of age, followed by a recovery at 12 months of age (two-way ANOVA: interaction: $P < 0.01$; Fig. 5c). Total Akt protein levels simultaneously decreased in 5-month-old HZ mice (Tukey's test: $P < 0.05$, Fig. 5c). Furthermore, the phosphorylation of Akt substrate GSK-3β at Serine 9 (p-GSK3β) was increased in the HZ group at 12 months compared to 5 months of age, indicating the inhibition of GSK-3β kinase (two-way ANOVA: interaction: $P < 0.01$; Fig. 5d). Additionally, the phosphorylation state of mTOR protein at Serine 2448, a downstream substrate of Akt, was significantly higher in 12-month-ol HZ mice compared to the younger group (two-way ANOVA: age effect: $P < 0.05$; Fig. 5e).

To investigate the impact of the PI3K/Akt signalling pathway on Tau protein, we examined the levels of phosphor-tau (AT8, AT100) and total tau in the hippocampus using western blot analysis at 5 and 12 months of age. In 12-month-old HZ mice, we observed a significant increase in tau phosphorylation at serine 202 and threonine 205 (p-Tau(S202/

T205)) compared to younger mice (one-way ANOVA: AT8/Tau Total: Tukey's test: $P < 0.05$,). This suggests that the phosphorylation of tau at these specific sites is influenced by the PI3K/Akt signalling pathway and may be associated with the pathological changes observed in 12-month-old HZ mice.

3.7. Dysregulation of peptide networks modulating insulin secretion and signalling in HTZ and HZ 5xFAD mice

Next, we evaluated the plasma levels of peptides involved in insulin release and signalling to assess insulin-linked metabolic pathways. In Fig. 6, we observed premature alterations of plasma hormone concentrations in 5-months-old 5xFAD transgenic mice. Most of this effect disappeared at 12 months old of age.

Statistical analysis revealed significant effects of genotype ($P < 0.01$) and age ($P < 0.05$). At 5 months of age, HZ mice had lower circulating plasma insulin levels compared to no-tg mice (Tukey's test: $P < 0.05$, Fig. 6a). This reduction in insulin levels was associated with decreased plasma levels of GIP, a potent stimulator of insulin secretion. Both HTZ and HZ mice at 5 months of age showed lower basal plasma levels of GIP compared to the age-matched no-tg group (two-way ANOVA: age effect: $P < 0.0001$, Tukey's test: $P < 0.05$, Fig. 6b). We also investigated the plasma levels of GLP1, another peptide involved in insulin-linked metabolic pathways that stimulated glucose-dependent insulin release. Two-way ANOVA revealed significant effects of genotype ($P < 0.05$) and age ($P < 0.01$). Post hoc comparison tests indicated a significant decrease in basal plasma levels of GLP-1 in HZ mice, which was more pronounced at 12 months of age (Tukey's test: $P < 0.05$, Fig. 6c).

In our analysis of hormones involved in the regulation of food intake and energy balance, we examined leptin and resistin levels in the plasma of 5xFAD transgenic and non-transgenic mice, considering the influence of sex (Quevedo et al., 1998; Roca et al., 1999). Leptin did not show dysregulation in plasma levels between 5xFAD transgenic and non-transgenic mice (Fig. 6d). Resistin, a peptide hormone associated with insulin sensitivity, displayed a 'genotype x age x sex' interaction (two-way ANOVA: $P < 0.01$) in circulating plasma levels. Post hoc analysis
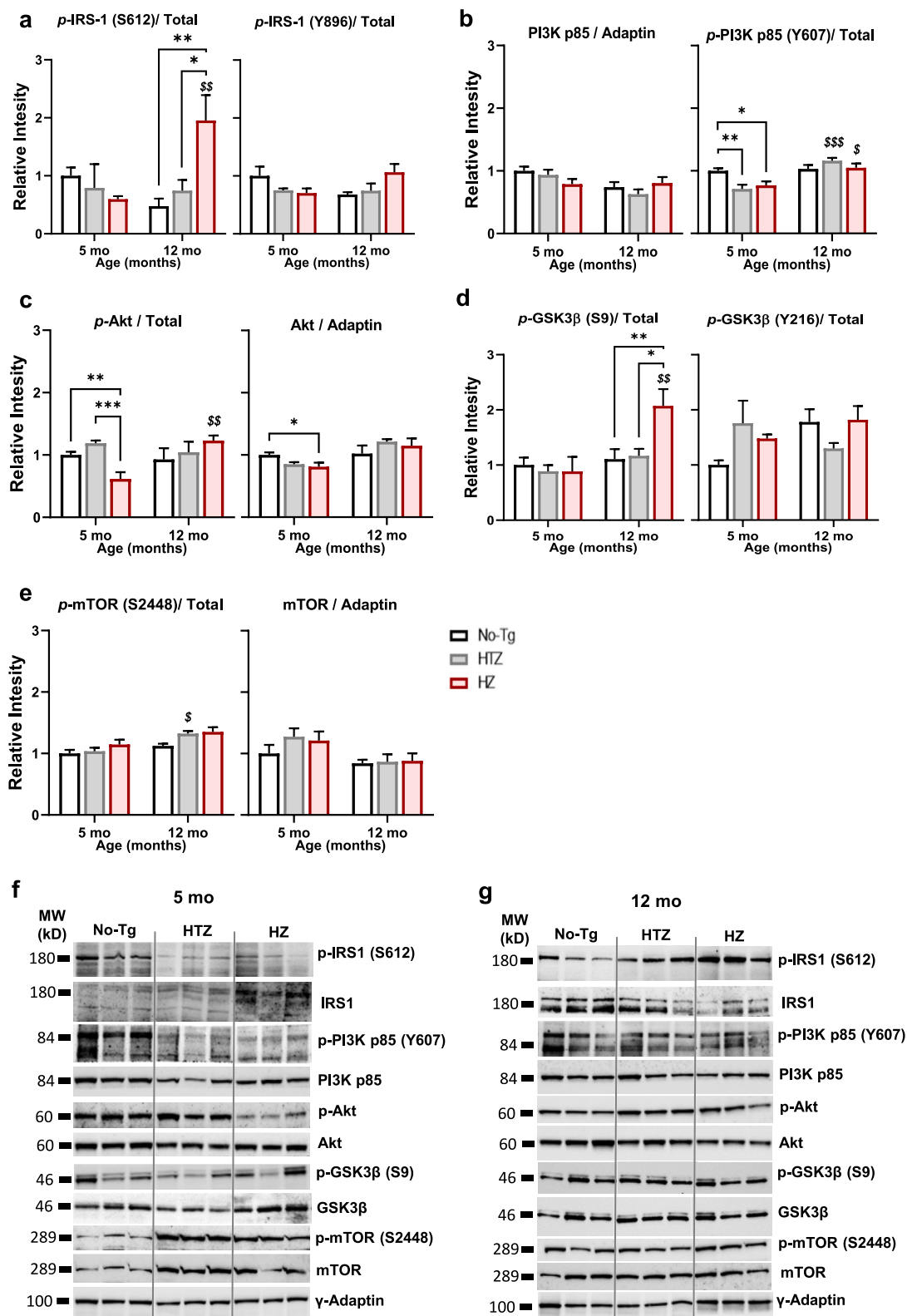
Fig. 5. The PI3-K/Akt pathway in the hippocampus of heterozygous and homozygous 5xFAD mice. Bar charts represent the relative intensity of protein expression of insulin receptor substrate 1 (IRS-1) phosphorylation at serine 612 and the amount of total IRS-1 (a), p85 regulatory domain of the phosphatidylinositol 3 kinase (p85-PI3K) phosphorylation at tyrosine 607, and quantity of total p85-PI3K (b). Protein Kinase B (Akt) phosphorylation on serine 473, and amount of total Akt (c). Glycogen synthase kinase 3β (GSK-3β) phosphorylation at serine 9, and amount of total GSK-3β (d). Mammalian Target of Rapamycin (mTOR) phosphorylation at serine 2448, and total mTOR € amount. The blots are a representation of all bands at 5 months (f), and 12 months (g) of age (See Supplementary Material S3 and S4 for additional information). The corresponding expression of γ-Adaptin is shown as a loading control per lane. All samples were obtained at the same time and processed in parallel. Histograms represent the mean ± SEM, $n = 6$. Bonferroni tests: difference between transgenic vs non-transgenic mice: (*) $P < 0.05$, (**) $P < 0.01$, (***) and $P < 0.001$; difference between 5- and 12- months age of the same genotype: ($) $P < 0.05$, ($$) $P < 0.01$, ($$$) $P < 0.001$.
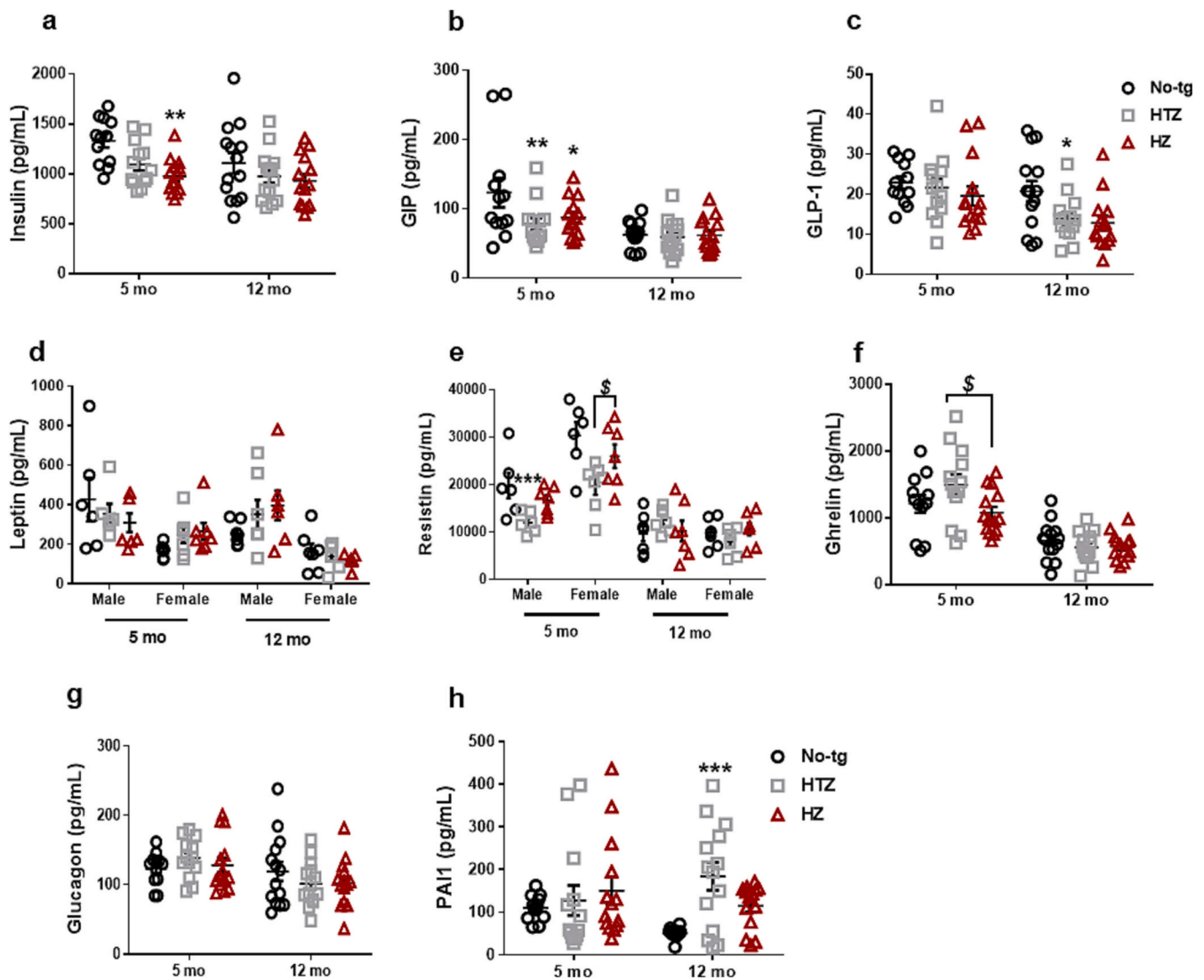
Fig. 6. . Insulin-linked metabolic pathways in heterozygous and homozygous 5xFAD mice. Plasma levels of insulin (a), gastric inhibitory polypeptide (GIP) (b), glucagon-like peptide-1 (GLP-1) (c), leptin (d), resistin (e), ghrelin (f), glucagon (g) and plasminogen activator inhibitor-1 (PAI-1) (h). All data represent the mean $\pm$ SEM, $n = 12$–14. Tukey's Test: difference between transgenic vs non-transgenic mice: (*) $P < 0.05$, (**) $P < 0.01$, (***) and $P < 0.001$; difference between HTZ and HZ condition: ($\$$) $P < 0.05$.

revealed lower resistin levels in both male and female HTZ mice compared to no-tg and HZ mice at 5 months of age (Tukey's test: $P < 0.05$, Fig. 6e).

In contrast, plasma ghrelin levels exhibited a significant age effect (two-way ANOVA: $P < 0.0001$). At 5 months of age, HZ mice displayed lower circulating ghrelin levels compared to HTZ mice (Tukey's test: $P < 0.05$, Fig. 6f). No significant differences in plasma glucagon levels were found between the genotypes at any age (Fig. 6g). PAI-1, a serine protease inhibitor involved in regulating blood clot clearance, demonstrated a significant effect of genotype ($P < 0.05$). Post hoc comparison analysis indicated increased PAI-1 level in the HTZ group compared to no-tg mice (Tukey's test: $P < 0.05$, Fig. 6h).

3.8. Altered gut microbiota composition in HZ mice with age

In our analysis of the gut microbiota composition, first we focused on the relative abundances of the *Firmicutes* and *Bacteroidetes* phyla. The *Firmicutes/Bacteroidetes* ratio, an important indicator of gut microbial balance, was significantly reduced in 12-month-old HZ compared to 5-month-old HZ (two-way ANOVA: age effect: $P < 0.0001$, Tukey's test: $P < 0.05$). This reduction was observed with age in all three genotypes,

but it was more pronounced in HZ mice (Fig. 7a).

Firmicutes are a large group of gram-positive bacteria that include species such as lactobacilli and clostridia. *Bacteroidetes*, on the other hand, are a smaller group of gram-negative bacteria that encompass bacteria like Bacteroides and Prevotella. The F/B ratio has been demonstrated to undergo alterations in patients with AD. In general, individuals with AD tend to exhibit a decreased proportion of *Firmicutes* and an elevated proportion of *Bacteroidetes*, which aligns with the findings from our study.

Additionally, we conducted a more in-depth taxonomic analysis. To accomplish this, we compared the taxonomic compositions obtained from the analyses of DNA sequences extracted from fecal microbiota samples using QIIME2. This comparison was performed at the family level in terms of relative abundance. Supplementary Material S6 displays abundance bars for each fecal sample. Significantly noticeable differences for the 'Genotype x Age' variables have predominantly been detected within eight families: *Prevotellaceae, Anaerovoracaceae, Defluviitaleaceae, Marinifilaceae, Lachnospiraceae, Saccharimonadaceae, Enterococcaceae,* and *Butyricicoccaceae*. *Prevotellaceae* and *Marinifilaceae* belong to the Phylum Bacteroidetes, Class Bacteroidia and Order Bacteroidales. *Anaerovoracaceae, Lachnospiraceae, Saccharimonadaceae*
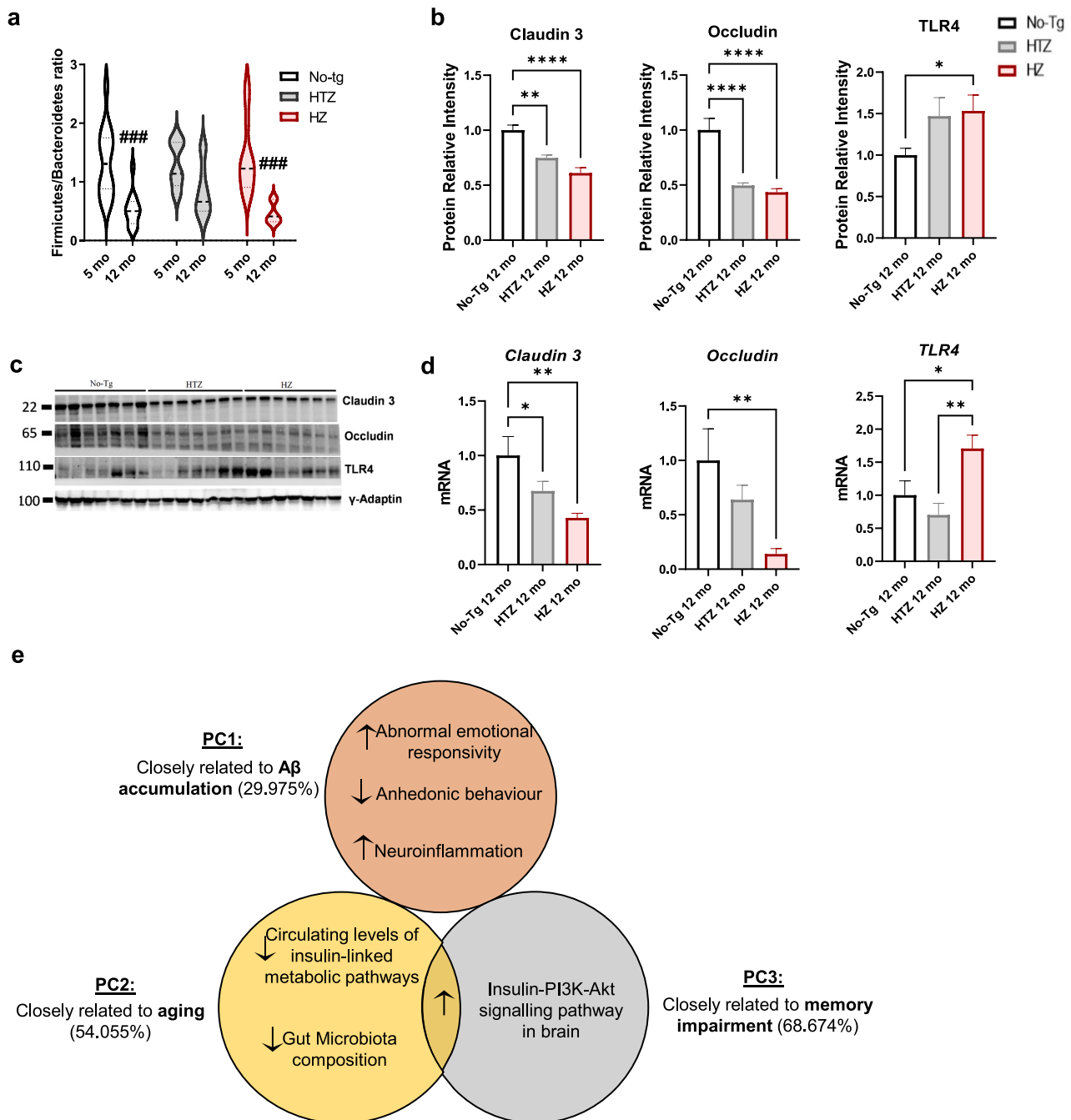
Fig. 7. Fecal microbiota compositions of heterozygous and homozygous 5xFAD mice and principal component analysis. The *Firmicutes/ Bacteroidetes* ratio (a). Bar charts represent the relative intensity of the protein expression of Claudin 3, Occludin and TLR4 in the small intestine tissue obtained at 12 months (b). The blots are representative pictures of Western blots of all bands (c) (See Supplementary Material S8 for additional information). Real-time PCR analysis for Claudin 3, Occludin and TLR4 in the small intestine tissue obtained from 12-month-old mice (d). Venn diagram showing exploratory principal component analysis (PCA) (e). Three principal components (PC) together explained 68.674% of the variance associated with Aβ accumulation, aging, and memory impairment. Histograms represent the mean ± SEM, n = 6. Tukey's Test: difference between non-transgenic vs transgenic mice t: (*) $P < 0.05$, (**) $P < 0.01$, (****) and $P < 0.001$; difference between aged group: (###) $P < 0.001$.

(formerly known as TM7) and *Butyricicoccaceae* belong to the Phylum Firmicutes, Class Clostridia, Order Clostridiales. Defluviitaleaceae even belonging to the Phylum Firmicutes and Class Clostridia, they are in the Order Eubacteriales. Enterococcaceae belong to the Phylum Firmicutes, Class Bacilli, Order Lactobacillales.

The graphs presented in Supplementary Material S6 illustrate the instances with the lowest *P*-values (< 0.05) between the variables of genotype and age. In relation to age, the percentage of relative abundance decreases in *Marinifilaceae, Lachnospiraceae*, and *Butyricicoccaceae*

($P < 0.05$) in all three genotypes. Conversely, it increases in *Saccharimonadaceae*, and *Enterococcaceae* ($P < 0.01$). At the genotype level, the abundance of *Prevotellaceae* in the no-tg group is significantly higher than in the transgenic groups ($P < 0.01$). Conversely, in *Anaerovoracaceae, Defluviitaleaceae*, and *Enterococcaceae*, the opposite is observed; the no-tg group exhibits lower levels compared to the transgenic groups ($P < 0.05$). Distinct differences between the two transgenic groups are identified in *Defluviitaleaceae, Marinifilaceae*, and *Butyricicoccaceae*: At 12 months, the abundance of *Defluviitaleaceae* in the HTZ group is

significantly lower than in HZ ($P < 0.01$). At 5 months, the abundance of *Marinifilaceae* is significantly higher in the HZ group ($P < 0.05$), whereas *Butyricicoccaceae* shows the opposite trend, being elevated in the HTZ group ($P < 0.05$).

3.9. Disruption of the small intestinal epithelial layer in HTZ and HZ mice with age

We analysed the expression of claudin 3, occludin, and Toll-Like Receptor 4 (TLR4) proteins in the small intestine, as well as their mRNA expression. At 5 months of age, no significant differences in the expression of claudin 3, occluding, and TLR4 were observed between the genotypes (Supplementary Material S7). However, at 12 months of age, significant changes were detected. The levels of claudin 3 and occluding, which are important proteins involved in maintaining the integrity of the intestinal barrier, decreased significantly in HTZ and HZ compared to age-matched no-tg mice (one-way ANOVA: Claudin 3: $P < 0.0001$, Tukey's test: $P < 0.05$, Occludin: $P < 0.0001$, Tukey's test: $P < 0.05$, Fig. 7b-c). In contrast, the levels of TLR4, a receptor involved in immune responses, were increased in HZ mice at 12 months of age compared to no-tg mice (one-way ANOVA: $P < 0.05$, Tukey's test: $P < 0.05$, Fig. 7b-c), suggesting an altered immune activation in the small intestine of HZ mice. These findings were supported by mRNA expression analysis (Fig. 7d), confirming the changes observed at the protein level.

3.10. Principal components analysis revealed that factors other than Aβ accumulation increase the risk of developing AD

We conducted a principal component analysis (PCA) to explore the relationship between cognitive impairment and the pathophysiological alterations observed in the 5xFAD transgenic animal model at both 5 and 12 months of age. The main results of the PCA are presented in Table S2, and the different profiles of the three genotypes are depicted in Fig. 7e. The PCA analysis revealed that the three components together accounted for 68.674% of the variance, allowing us to describe distinct profiles of the three genotypes. The first component, explaining 29.975% of the total variance, was associated with Aβ accumulation, as indicated by high factor loadings of Aβ_{40}, Aβ_{42}, and total Aβ. This component was also positively influenced by the time spent in the open arms of the EPM, and the presence of GFAP (a marker for astrocyte activation) and Iba1 (a marker for microglial activation). The second component, explaining 24.080% of the total variance, was primarily influenced by age and thus considered the aging component. This component was negatively loaded by factors related to insulin-linked metabolic pathways (resistin and ghrelin) and gut microbiota composition. On the other hand, it was positively loaded by factors associated with the insulin-PI3K-Akt signalling pathway (pGSK3 and pmTOR). The third component, explaining 14.619% of the variance, represented memory impairment. It was characterized by the performance in visual and acquisition learning phase of the MWM, a well-established test for assessing learning and memory. The insulin-PI3K-Akt signalling pathway (pIRS1) also positively influenced this component.

The PCA analysis provided insights into the relationship between cognitive impairment and the various pathophysiological alterations observed in the 5xFAD transgenic animal model. The components identified in the analysis represented Aβ accumulation, aging-related changes, and memory impairment (Fig. 7e). These findings contribute to our understanding of the complex interplay between molecular, metabolic, and cognitive factors in this model of neurodegenerative disease.

4. Discussion

Multiple studies using transgenic animal models like 5xFAD mice have focused on homozygous conditions to assess neurological deficiencies. However, few studies examined genetic load and age-

dependent neurodegenerative status (Richard et al., 2015). Here, using HTZ and HZ conditions, we showed that HZ has earlier and more severe cognitive dysfunction, despite neuropathological alterations to the HTZ group. Findings: 1) HZ animals showed more severe cognitive deficits than HTZ animals with age; 2) Both HTZ and HZ mice showed hippocampal dysfunction, including increased Aβ accumulation, neuroinflammation, and altered insulin-PI3K-Akt signalling; 3) HZ mice exhibited premature alterations of insulin-linked metabolic pathways, declining at 12 months of age regardless of genotype; 4) Altered gut microbiota associated with aging, more pronounced in HZ group; and 5) A disruption of the small intestinal epithelial layer in HTZ and HZ mice with age, which in turn is related to systemic inflammation.

We examined the behavioural phenotype of HTZ and HZ 5xFAD transgenic mice at two stages of AD: 5 months (early onset) and 12 months of age (middle onset). Anhedonia, characterized by a loss of interest or pleasure, is a core symptom in mood disorders like depression (Anisman and Zacharko, 1990) and has been associated with increased cortical Aβ load in AD patients (Babulal et al., 2016; Naudin et al., 2015; Reichman and Coyne, 1995). In rodents, sucrose/saccharin intake is commonly used to measure hedonic response (Scheggi et al., 2018; Strekalova et al., 2004). Our data showed that at 5 months of age, both HTZ and HZ mice showed reduced sucrose intake below the anhedonia criterion of 65% (Scheggi et al., 2018). These findings align with other AD mouse models, such as the 3xTg-AD model, which also exhibited depression-related behaviour and lower sucrose preference (Romano et al., 2014). However, some studies reported intact reward behaviour in 5xFAD mice, showing no variation in sucrose preference at early ages (Heckmann et al., 2019; Tang et al., 2016), as we observed in SacPT that saccharin consumption did not show a comparable change. This suggests that sucrose and saccharin solutions may produce different taste sensations and motivations for food in rodents (Nissenbaum and Sclafani, 1987; Sako et al., 1994) caused by glial activation and metabolic dysfunctions in the hypothalamus (López-Gambero et al., 2021). Alternative methods, such as submissive behaviour (Strekalova et al., 2004), or reduced sexual activity (Grønli et al., 2005), should be considered to better assess anhedonia in the 5xFAD model.

In the OP test, 12-month-old HZ mice exhibited anxiety-like behaviour by spending less time in the centre compared to HTZ and no-tg mice. However, in the EPM, both 5- and 12-month-old HZ mice spent more time in the open arms, avoiding the closed arms, which contradicted the expected behaviour. These paradoxical results may be attributed to sensorial deficits or abnormal vibrissal sensation in HZ mice, preventing them from assessing the risks of exposed arms in the EPM (narrow arm width, high illumination, and high height). Impaired sensory integration in 5xFAD mice (Flanigan et al., 2014) and early Aβ accumulation in the cortex, along with degeneration of layer V pyramidal neurons (Oakley et al., 2006), could explain this abnormal behaviour, which becomes more aversive with age. Previous reports have also described that 8-month-old HZ mice exhibited increased exploratory behaviour in the EPM, correlating with Aβ accumulation in the brain (Jawhar et al., 2012; Peters et al., 2013; Schneider et al., 2014), and suggesting disinhibitory tendencies similar to observed in AD patients (Jawhar et al., 2012).

In the present study, a noteworthy observation was made in the context of the cognitive performance of HTZ mice. While HZ mice exhibited significant impairments in hippocampal-dependent memory formation at 5 months of age, along with a more pronounced decline in cognitive function with advancing age, the cognitive trajectory of HTZ mice demonstrated a distinct pattern. Specifically, HTZ mice exhibited a dramatic memory deficit in the MWM at 5 months, which intriguingly showed a substantial recovery at 12 months. This unique cognitive profile in HTZ mice, marked by the disappearance of early deficits, introduces complexity to any direct age-based comparison between HTZ and HZ mice. Notably, HZ mice not only displayed memory deficits in the MWM but also demonstrated impairments in the Y-maze task, underscoring the consistent nature of their cognitive decline. In our

previous report, both 12-month-old HTZ and HZ mice displayed memory impairment in the novel object recognition (NOR) test (Medina-Vera et al., 2020). It is worth noting that while both tasks involve visual components, the NOR task encompasses a broader scope of recognition memory, which includes visual and perceptual discrimination. (Akkerman et al., 2012; Antunes and Biala, 2012; Dere et al., 2005). The MWM, on the other hand, assesses spatial learning and memory, as well as cognitive efficiency and flexibility (Gallagher et al., 1993; Morris et al., 1982). In this regard, 12-month-old HZ mice showed slower learning during the acquisition of spatial learning and impaired cognitive flexibility compared to HTZ and no-tg mice, consistent with a previous finding (Richard et al., 2015). Our findings illuminate the intricate relationship between genotype, task complexity, and cognitive performance, suggesting that deficits may emerge due to different processes or cognitive demands specific to each task. Though a few published studies have evaluated the impact of genetic load on cognitive function in the 5xFAD model, and behavioural data in this area remain limited.

While analysing both male and female animals together allowed us to draw broader insights into AD-related behaviours, we acknowledge that this approach might have obscured potential sex-specific effects. Future studies focused on sex-specific analyses are warranted to elucidate any differential behavioural phenotypes between male and female mice in the context of AD.

Homozygous 5xFAD mice exhibit Aβ accumulation (higher Aβ$_{42}$ deposition than Aβ$_{40}$) and neuronal loss in the hippocampus from 4 months of age (Oakley et al., 2006), especially in the CA1 region. Richard et al. (2015) described significant increases of extracellular plaque load in the cortex, hippocampus, and thalamus of 2-, 5- and 9-month-old HZ mice compared to age-matched HTZ mice. In addition, higher levels of soluble Aβ$_{42}$ were also observed in HZ mice at 2 months and 5 months of age (Richard et al., 2015). Our findings align with these studies, showing increased accumulation of Aβ$_{42}$-containing plaques in the DG, CA1, and CA3 regions of the hippocampus starting from 5 months of age, with greater accumulation in the CA1 area as they age compared to age-matched HTZ mice. Nevertheless, there was no age-related increase in Aβ$_{40}$-containing plaques in the hippocampus in either transgenic mouse model, potentially indicating a saturation effect (Oakley et al., 2006). Post-mortem studies in AD patients have highlighted significant amyloid deposition in the CA1 region of the hippocampus (Padurariu et al., 2012). This region plays a crucial role in information processing, receiving input from the DG via mossy fibers and projecting mainly to the subiculum, as well as being connected to the prefrontal cortex (Mu and Gage, 2011; Tzakis and Holahan, 2019). Reduced connectivity between the hippocampal CA1/subiculum and prefrontal cortex has been observed in AD patients (Allen et al., 2007). Further research is needed to investigate the degeneration and alterations in neural circuits associated with early Aβ accumulation. However, other factors, such as those shown in this study, may contribute to the pathological processes and clinical symptoms of AD. For instance, in our previous study, we demonstrated that there is an imbalance in the endocannabinoid system aggravated by transgenic load, which is related to memory dysfunction (Medina-Vera et al., 2020).

Given that some metabolic regulatory hormones play a role in controlling food intake, energy expenditure, and body weight (Friedman and Halaas, 1998; Schwartz et al., 2000), it is likely that metabolic alterations underlie to the difference in sucrose and saccharin consumption between HTZ and HZ 5xFAD mice. As revealed our previous research, both 6-month-old HTZ and HZ mice have lower body weight, food intake, and energy expenditure, indicating metabolic dysfunctions in the hypothalamus. These transgenic mice show decreased hypothalamic signalling of insulin and leptin, as well as reduced circulating levels and dysregulation in key metabolic sensors and neuropeptides involved in energy balance (López-Gambero et al., 2021). Consistent with these findings, our results demonstrate changes in insulin-related metabolic networks in HZT and HZ mice, particularly at 5 months of age. However, at 12 months of age, circulating levels of insulin-linked

metabolic hormones were reduced in three genotypes, suggesting an age-related decline independent of the specific genetic factors.

Increasing evidence suggests that AD is associated with alterations in brain energy metabolism (Cunnane et al., 2020). Human post-mortem (Rivera et al., 2005; Talbot et al., 2012) and clinical (Kim and Feldman, 2015; Ruegsegger et al., 2018) analyses have revealed brain insulin deficiency and insulin resistance in AD patients. Insulin and the PIK3-Akt protein pathway play important roles in neuronal growth and synapse formation (Gabbouj et al., 2019). Changes in the PI3K-Akt pathway arise predominantly as reduced phosphorylation or total levels of insulin-PI3K-Akt signalling cascade components. We observed decreased levels of PI3K and Akt at 5 months of age, but significantly higher protein expression at 12 months of age, possibly due to lipid product release by immune cells and subsequent activation of protein kinases, including Akt and GSK3β. In addition, as discussed below, the opening of the intestinal barrier and release of bacterial component like LPS may trigger neuroinflammation, supported by the role of TLR4 in mediating pro-inflammatory responses. Aβ oligomers were found to inhibit the Akt pathway (Mohamed et al., 2018), explaining their lower levels at 5 months of age and resulting in neuronal death. Post-mortem AD brain samples also showed decreased levels of the PI3K p85 subunit and Akt phosphorylation (Moloney et al., 2010; Steen et al., 2005). We found a decrease at 5 months of age, which may be attributed to increase Aβ and/or reduced plasma insulin levels, leading to decreased insulin-PI3K-Akt pathway signalling in the brain. Furthermore, elevated inhibitory serine phosphorylation of IRS1 at 12 months of age was associated with Aβ plaques and memory impairment, consistent with previous studies (Wang et al., 2019; Zheng and Wang, 2021). These findings indicate a link between the PI3K-Akt signalling pathway and memory deficits. Further research will be conducted to better understand the changes in GSK3β.

Given the nature of the 5xFAD model and its emphasis on Aβ-related processes, our investigation primarily aimed to explore the potential impact of the PI3K/Akt signalling pathway on Aβ production and associated pathogenesis. Although we did analyse tau phosphorylation as an additional measure. GSK-3β is a kinase known to phosphorylate tau and is closely linked to the insulin signalling cascade, regulated by Akt (Zhang et al., 2018) Our findings demonstrated the inhibition of GSK-3β in the hippocampus of 12-month-old HZ mice, along with the detection of tau protein phosphorylation at the same age. This activation may have been mediated by other tau kinases such as PKA, ERK1/2, or CDK5 (Medina-Vera et al., 2022). These results align with recent research (Medina-Vera et al., 2022), indicating that tau phosphorylation is regulated by p25/CDK5 kinase and rather than GSK-3β, as expected. In that study, the authors utilized the 3xTg AD tauopathy mouse model as a control, providing further evidence of CDK5 involvement in tau phosphorylation. In the present study, we explicitly acknowledge the limitations of our model in fully capturing tau pathology.

The activation of microglial cells and astrocytes in response to different forms of Aβ has attracted significant attention in the context of AD. In HZ mice, we observed increased expression of microglia and astrocytes starting from 5 months of age, accompanied by elevated Aβ accumulation in the hippocampus. This early neuroinflammatory response may contribute to the cognitive impairments observed in HZ mice. The activation of these cells can lead to the infiltration of blood cells into the CNS, particularly when there is biochemical or mechanical damage to the blood-brain barrier (BBB), resulting in altered permeability. Such events disrupt the exchange of substances between the CNS and the blood, leading to the loss of homeostatic functions, neuronal dysfunction, and damage (Bairamian et al., 2022). A major component affecting barrier disruption is the gut microbiota, whereby alterations along the brain-gut-microbiota axis may contribute significantly to the pathogenesis of AD (Bairamian et al., 2022; Kowalski and Mulak, 2019). For instance, the increased permeability of the intestinal barrier, caused by the disruption of tight junction proteins, allows microbial byproducts such as butyrate to reach the hippocampus and impact learning and

memory (Bourassa et al., 2016). Furthermore, gut microbiota-derived endotoxins like LPS can stimulate the immune system and CNS, influencing brain function (Bairamian et al., 2022; Kowalski and Mulak, 2019). In 12-month-old HZ 5xFAD mice, we observed alterations in gut microbiota composition, including a decrease in the *Firmicutes* phylum and an increase in the *Bacteroidetes* phylum. Additionally, we detected decreased expression of claudin 3 and occludin tight junction proteins, as well as increased expression of the TLR4 receptor in colon samples, indicating disruption of the small intestinal epithelial layer in both HTZ and HZ mice with age. This disruption could potentially facilitate the entry of inflammatory modulators or microbial products such as amyloidogenic peptides into the brain, exacerbating the symptoms of AD (Zhao et al., 2015). Different studies have reported conflicting results regarding the *Firmicutes* and *Bacteroidetes* populations in the context of AD. Shukla et al. (2021) found a decrease in *Firmicutes* and an increase in *Bacteroidetes* populations associated with peripheral inflammation (Shukla et al., 2021), while other observed the opposite pattern or different alterations in male HZ 5xFAD mice at 9 months of age (Brandscheid et al., 2017). In AD patient, Vogt et al. (2017) showed a decrease in *Firmicutes* and an increase in *Bacteroidetes* in fecal samples from AD participants compared to healthy participants (Vogt et al., 2017), and other studies have also demonstrated a reduction in *Firmicutes* and an increase in *Proteobacteria* in AD patients compared to healthy participants (Chandra et al., 2023). These microbial populations have been linked to insulin resistance, increased Aβ deposition, and the release of pro-inflammatory cytokines triggered by LPS, indicating their potential involvement in AD pathogenesis (Bairamian et al., 2022; Kowalski and Mulak, 2019). The primary disparities revealed by the family analysis predominantly manifest in the context of age-related comparisons. Among the families that were differentially present in the gut microbiota of 5XFD mice, *Lachnospiraceae* and *Enterococcaceae* have been described to be differentially present in human patients of AD. Other families such as *Prevotellaceae* are butyrate-producing genera associated with Alzheimer's disease in specific *APOE* genotypes (Tran et al., 2019; Zhuang et al., 2018), while *Marinifilaceae* was closely related to specific fecal fatty acids and serum glycerolipids dysregulated in the triple transgenic AD mouse model (Cheng et al., 2022). Noteworthy genotype-specific differences surface between the non-tg and transgenic specimens at 5 months of age. However, these distinctions between genotypes fade by 12 months, suggesting the potential of these fecal microbiota families as early-age markers for AD identification. More specifically, we suggest that *Enterococcaceae* could be significantly impacted by both age and genotype. It shows a noteworthy increase at 12 months compared to 5 months of age, and it's more prominent in the transgenic groups compared to the no-tg group. These last results underscore the complexity of the gut-brain axis and provides valuable insights into potential links between gut microbiota and AD pathogenesis.

4.1. Limitations

The present study helped to further characterize this relevant animal model of AD. However, a crucial aspect that need to be developed is to describe how these factors contribute to individual development of the disease, using as an end point the cognitive impairment, to identify potential interventions that might slow disease progression in vulnerable subjects. The controlled addition of risk factors such as APOE4 (by using the EFAD-TG, a 5XFAD mouse overexpressing human APOE4) (D. S. Liu et al., 2015), diet or microbiome alterations, will indeed help in the future to further delimitate the new type of interventions/treatments that eventually may improve the clinical course of AD patients at early stages. An important additional limitation for the present results derives from the use of a transgenic approach that might generate insertional mutagenesis by the transgenes. Although this has not been found in 5xFAD transgenes, it is not possible to rule out impacts on noncoding regulatory sequences such as enhancers, insulators, or secondary structures.

5. Conclusion

In summary, our study comprehensively characterizes the behavioural, physiological, and gut microbiota phenotypes in HTZ and HZ 5xFAD mice across two stages of AD. We found that the genetic load in HZ mice leads to more severe cognitive impairment and specific metabolic alterations compared to HTZ mice. Importantly, impaired cognition in the 5xFAD mouse model is not solely determined by the Aβ burden in the brain, particularly in the hippocampus. Our findings shed light on the complex nature of AD as a neurodegenerative disease, highlighting the interplay between insulin resistance, increased Aβ deposition, and the gut microbiome. These insights provide a deeper understanding of the disease and offer potential avenues for developing new therapeutic strategies targeting these interconnected factors.

Author contributions

Fernando Rodríguez de Fonseca, Luis J. Santín, and Cristina Rosell-Valle were responsible for the study concept and design. Dina Medina-Vera, Cristina Rosell-Valle, Emma Noelia Zambrana-Infante, and Antonio J. López-Gambero performed animal experiments and histology. Julia Verheul performed microbiota analysis. Cristina Rosell-Valle and Dina Medina-Vera contributed to data collection and/or interpretation and performed the statistical analyses reviewed by Juan Suárez, Francisco J. Pavón, and Elena Baixeras. The first draft of the manuscript was written by Cristina Rosell-Valle and Dina Medina-Vera; all authors commented on previous versions of the manuscript. All authors critically reviewed the content and approved the final manuscript for publication.

Declaration of Competing Interest

The authors have no relevant financial or non-financial interests to disclose.

Data availability

All data generated or analysed during this study are included in this published article and its supplementary information files. Raw data are available upon reasonable request from the corresponding author.

Acknowledgements

Appendix A. Supplementary data

Supplementary data to this article can be found online at https://doi.org/10.1016/j.nbd.2023.106295.

References

Akkerman, S., Blokland, A., Reneerkens, O., van Goethem, N.P., Bollen, E., Gijselaers, H. J.M., Lieben, C.K.J., Steinbusch, H.W.M., Prickaerts, J., 2012. Object recognition testing: methodological considerations on exploration and discrimination measures. Behav. Brain Res. 232 (2), 335–347. https://doi.org/10.1016/J.BBR.2012.03.022.

Allen, G., Barnard, H., McColl, R., Hester, A.L., Fields, J.A., Weiner, M.F., Ringe, W.K., Lipton, A.M., Brooker, M., McDonald, C., Cullum, C.M., 2007. Reduced hippocampal functional connectivity in Alzheimer disease. Arch. Neurol. 64 (10), 1482–1487. https://doi.org/10.1001/ARCHNEUR.64.10.1482.

Anisman, H., Zacharko, R.M., 1990. Multiple neurochemical and behavioral consequences of stressors: implications for depression. Pharmacol. Ther. 46 (1), 119–136. https://doi.org/10.1016/0163-7258(90)90039-5.

Antunes, M., Biala, G., 2012. The novel object recognition memory: neurobiology, test procedure, and its modifications. Cogn. Process. 13 (2), 93–110. https://doi.org/10.1007/S10339-011-0430-Z.

Babulal, G.M., Ghoshal, N., Head, D., Vernon, E.K., Holtzman, D.M., Benzinger, T.L.S., Fagan, A.M., Morris, J.C., Roe, C.M., 2016. Mood changes in cognitively normal older adults are linked to Alzheimer's disease biomarker levels. Am. J. Geriatr. Psychiatry 24 (11), 1095. https://doi.org/10.1016/J.JAGP.2016.04.004.

Bairamian, D., Sha, S., Rolhion, N., Sokol, H., Dorothée, G., Lemere, C.A., Krantic, S., 2022. Microbiota in neuroinflammation and synaptic dysfunction: a focus on Alzheimer's disease. Mol. Neurodegener. 17 (1), 1–23. https://doi.org/10.1186/S13024-022-00522-2.

Banks, W.A., 2008. The blood-brain barrier: connecting the gut and the brain. Regul. Pept. 149 (1–3), 11–14. https://doi.org/10.1016/J.REGPEP.2007.08.027.

Bartholomew, A., Sturgeon, C., Siatskas, M., Ferrer, K., McIntosh, K., Patil, S., Hardy, W., Devine, S., Ucker, D., Deans, R., Moseley, A., Hoffman, R., 2002. Mesenchymal stem cells suppress lymphocyte proliferation in vitro and prolong skin graft survival in vivo. Exp. Hematol. 30 (1), 42–48. https://doi.org/10.1016/S0301-472X(01)00769-X.

Bass, J.J., Wilkinson, D.J., Rankin, D., Phillips, B.E., Szewczyk, N.J., Smith, K., Atherton, P.J., 2017. An overview of technical considerations for Western blotting applications to physiological research. Scand. J. Med. Sci. in Sports 27 (1), 4–25. https://doi.org/10.1111/SMS.12702.

Bekris, L.M., Yu, C.E., Bird, T.D., Tsuang, D.W., 2010. Genetics of Alzheimer disease. J. Geriatr. Psychiatry Neurol. 23 (4), 213–227. https://doi.org/10.1177/0891988710383571.

Bird, C.M., BuBird, C.M., Burgess, N., 2008. The hippocampus and memory: insights from spatial processing. Nat. Rev. Neurosci. 9 (3), 182–194. https://doi.org/10.1038/NRN2335.

Bokulich, N.A., Kaehler, B.D., Rideout, J.R., Dillon, M., Bolyen, E., Knight, R., Huttley, G. A., Gregory Caporaso, J., 2018. Optimizing taxonomic classification of marker-gene amplicon sequences with QIIME 2's q2-feature-classifier plugin. Microbiome 6 (1), 1–17. https://doi.org/10.1186/s40168-018-0470-z.

Bolyen, E., Rideout, J.R., Dillon, M.R., Bokulich, N.A., Abnet, C.C., Al-Ghalith, G.A., Alexander, H., Alm, E.J., Arumugam, M., Asnicar, F., Bai, Y., Bisanz, J.E., Bittinger, K., Brejnrod, A., Brislawn, C.J., Brown, C.T., Callahan, B.J., Caraballo-Rodríguez, A.M., Chase, J., Caporaso, J.G., 2019. Reproducible, interactive, scalable and extensible microbiome data science using QIIME 2. Nat. Biotechnol. 37 (8), 852–857. https://doi.org/10.1038/s41587-019-0209-9.

Bourassa, M.W., Alim, I., Bultman, S.J., Ratan, R.R., 2016. Butyrate, neuroepigenetics and the gut microbiome: can a high fiber diet improve brain health? Neurosci. Lett. 625, 56. https://doi.org/10.1016/J.NEULET.2016.02.009.

Braak, H., Braak, E., 1991. Demonstration of amyloid deposits and neurofibrillary changes in whole brain sections. Brain Pathol. 1 (3), 213–216. https://doi.org/10.1111/J.1750-3639.1991.tb00661.x.

Brandscheid, C., Schuck, F., Reinhardt, S., Schäfer, K.H., Pietrzik, C.U., Grimm, M., Hartmann, T., Schwiertz, A., Endres, K., 2017. Altered gut microbiome composition and tryptic activity of the 5xFAD Alzheimer's mouse model. J. Alzheimers Dis. 56 (2), 775–788. https://doi.org/10.3233/JAD-160926.

Braniste, V., Al-Asmakh, M., Kowal, C., Anuar, F., Abbaspour, A., Tóth, M., Korecka, A., Bakocevic, N., Guan, N.L., Kundu, P., Gulyás, B., Halldin, C., Hultenby, K., Nilsson, H., Hebert, H., Volpe, B.T., Diamond, B., Pettersson, S., 2014. The gut microbiota influences blood-brain barrier permeability in mice. Sci. Transl. Med. 6 (263) https://doi.org/10.1126/SCITRANSLMED.3009759.

Bronzuoli, M.R., Facchinetti, R., Valenza, M., Cassano, T., Steardo, L., Scuderi, C., 2019. Astrocyte function is affected by aging and not Alzheimer's disease: a preliminary investigation in hippocampi of 3xTg-AD mice. Front. Pharmacol. 10 https://doi.org/10.3389/FPHAR.2019.00644.

Callahan, B.J., McMurdie, P.J., Rosen, M.J., Han, A.W., Johnson, A.J.A., Holmes, S.P., 2016. DADA2: high-resolution sample inference from Illumina amplicon data. Nat. Methods 13 (7), 581–583. https://doi.org/10.1038/nmeth.3869.

Castilla-Ortega, E., Hoyo-Becerra, C., Pedraza, C., Chun, J., RodrÂ-guez De Fonseca, F., Estivill-TorrÂos, G., SantÂ-n, L.J., 2011. Correction: Aggravation of Chronic Stress Effects on Hippocampal Neurogenesis and Spatial Memory in LPA 1 Receptor Knockout Mice. PLoS ONE 6 (11), e25522. https://doi.org/10.1371/annotation/c105dab8-59b8-467a-9223-5bd92936e49a.

Chandra, S., Sisodia, S.S., Vassar, R.J., 2023. The gut microbiome in Alzheimer's disease: what we know and what remains to be explored. Mol. Neurodegener. 18 (1) https://doi.org/10.1186/S13024-023-00595-7.

Cheng, X., Tan, Y., Li, H., Huang, J., Zhao, D., Zhang, Z., Yi, M., Zhu, L., Hui, S., Yang, J., Peng, W., 2022. Fecal 16S rRNA sequencing and multi-compartment metabolomics revealed gut microbiota and metabolites interactions in APP/PS1 mice. Comput. Biol. Med. 151, 106312. https://doi.org/10.1016/J.COMPBIOMED.2022.106312.

Cho, W.H., Park, J.C., Chung, C.H., Jeon, W.K., Han, J.S., 2014. Learning strategy preference of 5XFAD transgenic mice depends on the sequence of place/spatial and cued training in the water maze task. Behav. Brain Res. 273, 116–122. https://doi.org/10.1016/J.BBR.2014.07.033.

Cryan, J.F., Dinan, T.G., 2012. Mind-altering microorganisms: the impact of the gut microbiota on brain and behaviour. Nat. Rev. Neurosci. 13 (10), 701–712. https://doi.org/10.1038/nrn3346.

Cunnane, S.C., Trushina, E., Morland, C., Prigione, A., Casadesus, G., Andrews, Z.B., Beal, M.F., Bergersen, L.H., Brinton, R.D., de la Monte, S., Eckert, A., Harvey, J., Jeggo, R., Jhamandas, J.H., Kann, O., la Cour, C.M., Martin, W.F., Mithieux, G., Moreira, P.I., Millan, M.J., 2020. Brain energy rescue: an emerging therapeutic concept for neurodegenerative disorders of ageing. Nat. Rev. Drug Discov. 19 (9), 609–633. https://doi.org/10.1038/S41573-020-0072-X.

Dere, E., Huston, J.P., De Souza Silva, M.A., 2005. Integrated memory for objects, places, and temporal order: evidence for episodic-like memory in mice. Neurobiol. Learn. Mem. 84 (3), 214–221. https://doi.org/10.1016/J.NLM.2005.07.002.

Flanigan, T.J., Xue, Y., Rao, S.K., Dhanushkodi, A., McDonald, M.P., 2014. Abnormal vibrissa-related behavior and loss of barrel field inhibitory neurons in 5xFAD transgenics. Genes Brain Behav. 13 (5), 488–500. https://doi.org/10.1111/gbb.12133.

Friedman, J.M., Halaas, J.L., 1998. Leptin and the regulation of body weight in mammals. Nature 395 (6704), 763–770. https://doi.org/10.1038/27376.

Furcila, D., Defelipe, J., Alonso-Nanclares, L., 2018. A study of amyloid-β and Phosphotau in plaques and neurons in the Hippocampus of Alzheimer's disease patients. J. Alzheimer's Dis. 64 (2), 417–435. https://doi.org/10.3233/JAD-180173.

Gabbouj, S., Ryhänen, S., Marttinen, M., Wittrahm, R., Takalo, M., Kemppainen, S., Martiskaine, H., Tanila, H., Haapasalo, A., Hiltunen, M., Natunen, T., 2019. Altered insulin signaling in Alzheimer's disease brain-special emphasis on pi3k-akt pathway. Front. Neurosci. 13 (JUN), 629. https://doi.org/10.3389/FNINS.2019.00629/BIBTEX.

Gallagher, M., Burwell, R., Burchinal, M.R., 1993. Severity of spatial learning impairment in aging: development of a learning index for performance in the Morris water maze. Behav. Neurosci. 107 (4), 618–626. https://doi.org/10.1037/0735-7044.107.4.618.

Girard, S.D., Jacquet, M., Baranger, K., Migliorati, M., Escoffier, G., Bernard, A., Khrestchatisky, M., Féron, F., Rivera, S., Roman, F.S., Marchetti, E., 2014. Onset of hippocampus-dependent memory impairments in 5XFAD transgenic mouse model of Alzheimer's disease. Hippocampus 24 (7), 762–772. https://doi.org/10.1002/HIPO.22267.

Grønli, J., Murison, R., Fiske, E., Bjorvatn, B., Sørensen, E., Portas, C.M., Ursin, R., 2005. Effects of chronic mild stress on sexual behavior, locomotor activity and consumption of sucrose and saccharine solutions. Physiol. Behav. 84 (4), 571–577. https://doi.org/10.1016/J.PHYSBEH.2005.02.007.

Hammer, L.R., 1967. Saccharin and sucrose intake Long-and short-term tests. J. Psychon. Sci. 8, 367–368.

Hardy, J., Selkoe, D.J., 2002. The amyloid hypothesis of Alzheimer's disease: progress and problems on the road to therapeutics. Science (New York, N.Y.) 297 (5580), 353–356. https://doi.org/10.1126/SCIENCE.1072994.

Heckmann, B.L., Teubner, B.J.W., Tummers, B., Guy, C.S., Zakharenko, S.S., Green Correspondence, D.R., 2019. LC3-associated endocytosis facilitates β-amyloid clearance and mitigates neurodegeneration in murine Alzheimer's disease. Cell 178, 536–551 e14. https://doi.org/10.1016/j.cell.2019.05.056.

Hsiao, K., Chapman, P., Nilsen, S., Eckman, C., Harigaya, Y., Younkin, S., Yang, F., Cole, G., 1996. Correlative memory deficits, Abeta elevation, and amyloid plaques in transgenic mice. Science (New York, N.Y.) 274 (5284), 99–102. https://doi.org/10.1126/SCIENCE.274.5284.99.

Jawhar, S., Trawicka, A., Jenneckens, C., Bayer, T.A., Wirths, O., 2012. Motor deficits, neuron loss, and reduced anxiety coinciding with axonal degeneration and intraneuronal Aβ aggregation in the 5XFAD mouse model of Alzheimer's disease. Neurobiol. Aging 33 (1). https://doi.org/10.1016/J.NEUROBIOLAGING.2010.05.027, 196.e29-196.e40.

Kilkenny, C., Browne, W.J., Cuthill, I.C., Emerson, M., Altman, D.G., 2010. Improving bioscience research reporting: The arrive guidelines for animal research. PLoS Biology 8 (6). https://doi.org/10.1371/journal.pbio.1000412.

Kim, B., Feldman, E.L., 2015. Insulin resistance as a key link for the increased risk of cognitive impairment in the metabolic syndrome. Exp. Mol. Med. 47 (3), e149 https://doi.org/10.1038/EMM.2015.3.

Kimura, R., Ohno, M., 2009. Impairments in remote memory stabilization precede hippocampal synaptic and cognitive failures in 5XFAD Alzheimer mouse model. Neurobiol. Dis. 33 (2), 229–235. https://doi.org/10.1016/J.NBD.2008.10.006.

Kowalski, K., Mulak, A., 2019. Brain-gut-microbiota axis in Alzheimer's disease. J. Neurogastroenterol. Motil. 25 (1), 48. https://doi.org/10.5056/JNM18087.

Ledesma, J.C., Rodríguez-Arias, M., Gavito, A.L., Sánchez-Pérez, A.M., Viña, J., Medina Vera, D., Rodríguez de Fonseca, F., Miñarro, J., 2021. Adolescent binge-ethanol accelerates cognitive impairment and β-amyloid production and dysregulates endocannabinoid signaling in the hippocampus of APP/PSE mice. Addict. Biol. 26 (1) https://doi.org/10.1111/ADB.12883.

Levy-Lahad, E., Wasco, W., Poorkaj, P., Romano, D.M., Oshima, J., Pettingell, W.H., Yu, C.E., Jondro, P.D., Schmidt, S.D., Wang, K., Crowley, A.C., Fu, Y.H., Guenette, S. Y., Galas, D., Nemens, E., Wijsman, E.M., Bird, T.D., Schellenberg, G.D., Tanzi, R.E., 1995. Candidate gene for the chromosome 1 familial Alzheimer's disease locus. Science (New York, N.Y.) 269 (5226), 973–977. https://doi.org/10.1126/SCIENCE.7638622.

Liao, H.Y., Wang, Z. Qiang, Da, C.M., Zhou, K.S., Zhang, H. Hong, 2022. Ski regulates proliferation and migration of reactive astrocytes induced by lipopolysaccharide

(LPS) through PI3K/Akt pathway. J. Neuroimmunol. 364 https://doi.org/10.1016/j.jneuroim.2022.577807.

Liu, J., Li, L., 2019. Targeting autophagy for the treatment of Alzheimer's disease: challenges and opportunities. Front. Mol. Neurosci. 12, 203. https://doi.org/10.3389/FNMOL.2019.00203/BIBTEX.

Liu, D.S., Pan, X.D., Zhang, J., Shen, H., Collins, N.C., Cole, A.M., Koster, K.P., Ben Aissa, M., Dai, X.M., Zhou, M., Tai, L.M., Zhu, Y.G., Ladu, M.J., Chen, X.C., 2015. APOE4 enhances age-dependent decline in cognitive function by down-regulating an NMDA receptor pathway in EFAD-Tg mice. Mol. Neurodegener. 10 (1) https://doi.org/10.1186/s13024-015-0002-2.

Logsdon, A.F., Erickson, M.A., Rhea, E.M., Salameh, T.S., Banks, W.A., 2018. Gut reactions: how the blood-brain barrier connects the microbiome and the brain. Exp. Biol. Med. (Maywood, N.J.) 243 (2), 159–165. https://doi.org/10.1177/1535370217743766.

Long, H.Z., Cheng, Y., Zhou, Z.W., Luo, H.Y., Wen, D.D., Gao, L.C., 2021. PI3K/AKT signal pathway: a target of natural products in the prevention and treatment of Alzheimer's disease and Parkinson's disease. Front. Pharmacol. 12 https://doi.org/10.3389/FPHAR.2021.648636/FULL.

López-Gambero, A.J., Rosell-Valle, C., Medina-Vera, D., Navarro, J.A., Vargas, A., Rivera, P., Sanjuan, C., Rodríguez de Fonseca, F., Suárez, J., 2021. A negative energy balance is associated with metabolic dysfunctions in the hypothalamus of a humanized preclinical model of Alzheimer's disease, the 5XFAD mouse. Int. J. Mol. Sci. 22 (10), 5365. https://doi.org/10.3390/IJMS22105365.

Medina-Vera, D., Rosell-Valle, C., López-Gambero, A.J., Navarro, J.A., Zambrana-Infantes, E.N., Rivera, P., Santín, L.J., Suarez, J., de Fonseca, F.R., 2020. Imbalance of endocannabinoid/lysophosphatidylinositol receptors marks the severity of alzheimer's disease in a preclinical model: a therapeutic opportunity. Biology 9 (11), 1–22. https://doi.org/10.3390/biology9110377.

Medina-Vera, D., Navarro, J.A., Rivera, P., Rosell-Valle, C., Gutiérrez-Adán, A., Sanjuan, C., López-Gambero, A.J., Tovar, R., Suárez, J., Pavón, F.J., Baixeras, E., Decara, J., Rodríguez de Fonseca, F., 2022. d-Pinitol promotes tau dephosphorylation through a cyclin-dependent kinase 5 regulation mechanism: a new potential approach for tauopathies? Br. J. Pharmacol. 179 (19), 4655. https://doi.org/10.1111/BPH.15907.

Miedel, C.J., Patton, J.M., Miedel, A.N., Miedel, E.S., Levenson, J.M., 2017. Assessment of spontaneous alternation, novel object recognition and limb clasping in transgenic mouse models of amyloid-β and tau neuropathology. J. Vis. Exp. 2017 (123) https://doi.org/10.3791/55523.

Milstein, J.L., Ferris, H.A., 2021. The brain as an insulin-sensitive metabolic organ. Mol. Metab. 52 https://doi.org/10.1016/J.MOLMET.2021.101234.

Mohamed, A., Viveiros, A., Williams, K., De Chaves, E.P., 2018. Aβ inhibits SREBP-2 activation through Akt inhibition. J. Lipid Res. 59 (1), 1–13. https://doi.org/10.1194/jlr.M076703.

Moloney, A.M., Griffin, R.J., Timmons, S., O'Connor, R., Ravid, R., O'Neill, C., 2010. Defects in IGF-1 receptor, insulin receptor and IRS-1/2 in Alzheimer's disease indicate possible resistance to IGF-1 and insulin signalling. Neurobiol. Aging 31 (2), 224–243. https://doi.org/10.1016/J.NEUROBIOLAGING.2008.04.002.

Morris, R.G.M., Garrud, P., Rawlins, J.N.P., O'Keefe, J., 1982. Place navigation impaired in rats with hippocampal lesions. Nature 297 (5868), 681–683. https://doi.org/10.1038/297681a0.

Mu, Y., Gage, F.H., 2011. Adult hippocampal neurogenesis and its role in Alzheimer's disease. Mol. Neurodegener. 6 (1), 1–9. https://doi.org/10.1186/1750-1326-6-85/TABLES/1.

Naudin, M., Mondon, K., El-Hage, W., Perriot, E., Boudjarane, M., Desmidt, T., Lorette, A., Belzung, C., Hommet, C., Atanasova, B., 2015. Taste identification used as a potential discriminative test among depression and Alzheimer's disease in elderly: A pilot study. Psychiatry Res. 228 (2), 228–232. https://doi.org/10.1016/J.PSYCHRES.2015.03.021.

Nissenbaum, J.W., Sclafani, A., 1987. Qualitative differences in polysaccharide and sugar tastes in the rat: a two-carbohydrate taste model. Neurosci. Biobehav. Rev. 11 (2), 187–196. https://doi.org/10.1016/S0149-7634(87)80025-8.

Oakley, H., Cole, S.L., Logan, S., Maus, E., Shao, P., Craft, J., Guillozet-Bongaarts, A., Ohno, M., Disterhoft, J., Van Eldik, L., Berry, R., Vassar, R., 2006. Intraneuronal β-amyloid aggregates, neurodegeneration, and neuron loss in transgenic mice with five familial Alzheimer's disease mutations: potential factors in amyloid plaque formation. J. Neurosci. 26 (40), 10129–10140. https://doi.org/10.1523/JNEUROSCI.1202-06.2006.

O'Neill, C., 2013. PI3-kinase/Akt/mTOR signaling: impaired on/off switches in aging, cognitive decline and Alzheimer's disease. Exp. Gerontol. 48 (7), 647–653. https://doi.org/10.1016/J.EXGER.2013.02.025.

Ott, A., Stolk, R.P., Van Harskamp, F., Pols, H.A.P., Hofman, A., Breteler, M.M.B., 1999. Diabetes mellitus and the risk of dementia: the Rotterdam study. Neurology 53 (9), 1937–1942. https://doi.org/10.1212/WNL.53.9.1937.

Padurariu, M., Ciobica, A., Mavroudis, I., Fotiou, D., Baloyannis, S., 2012. Hippocampal neuronal loss in the CA1 and CA3 areas of Alzheimer's disease patients. Psychiatr. Danub. 24 (2), 152–158.

Peters, O.M., Shelkovnikova, T., Tarasova, T., Springe, S., Kukharsky, M.S., Smith, G.A., Brooks, S., Kozin, S.A., Kotelevtsev, Y., Bachurin, S.O., Ninkina, N., Buchmana, V.L., 2013. Chronic Administration of Dimebon does not ameliorate amyloid-β pathology in 5xFAD transgenic mice. J. Alzheimers Dis. 36 (3), 589–596. https://doi.org/10.3233/JAD-130071.

Quast, C., Pruesse, E., Yilmaz, P., Gerken, J., Schweer, T., Yarza, P., Peplies, J., Glöckner, F.O., 2013. The SILVA ribosomal RNA gene database project: improved data processing and web-based tools. Nucleic Acids Res. 41 (D1) https://doi.org/10.1093/nar/gks1219.

Quevedo, S., Roca, P., Picó, C., Palou, A., 1998. Sex-associated differences in cold-induced UCP1 synthesis in rodent brown adipose tissue. Pflugers Arch. - Eur. J. Physiol. 436 (5), 689–695. https://doi.org/10.1007/S004240050690.

Razani, E., Pourbagheri-Sigaroodi, A., Safaroghli-Azar, A., Zoghi, A., Shanaki-Bavarsad, M., Bashash, D., 2021. The PI3K/Akt signaling axis in Alzheimer's disease: a valuable target to stimulate or suppress? Cell Stress Chaperones 26 (6), 871–887. https://doi.org/10.1007/s12192-021-01231-3.

Reichman, W.E., Coyne, A.C., 1995. Depressive symptoms in Alzheimer's disease and multi-infarct dementia. J. Geriatr. Psychiatry Neurol. 8 (2), 96–99. https://doi.org/10.1177/089198879500800203.

Richard, B.C., Kurdakova, A., Baches, S., Bayer, T.A., Weggen, S., Wirths, O., 2015. Gene dosage dependent aggravation of the neurological phenotype in the 5XFAD mouse model of Alzheimer's disease. J. Alzheimers Dis. 45 (4), 1223–1236. https://doi.org/10.3233/JAD-143120.

Rivera, E.J., Goldin, A., Fulmer, N., Tavares, R., Wands, J.R., De La Monte, S.M., 2005. Insulin and insulin-like growth factor expression and function deteriorate with progression of Alzheimer's disease: link to brain reductions in acetylcholine. J. Alzheimer's Dis. 8 (3), 247–268. https://doi.org/10.3233/JAD-2005-8304.

Roca, P., Rodriguez, A.M., Oliver, P., Bonet, M.L., Quevedo, S., Picó, C., Palou, A., 1999. Brown adipose tissue response to cafeteria diet-feeding involves induction of the UCP2 gene and is impaired in female rats as compared to males. Pflugers Arch. - Eur. J. Physiol. 438 (5), 628–634. https://doi.org/10.1007/S004249900107.

Rogaev, E.I., Sherrington, R., Rogaeva, E.A., Levesque, G., Ikeda, M., Liang, Y., Chi, H., Lin, C., Holman, K., Tsuda, T., Mar, L., Sorbi, S., Nacmias, B., Piacentini, S., Amaducci, L., Chumakov, I., Cohen, D., Lannfelt, L., Fraser, P.E., George-Hyslop, P. H.S., 1995. Familial Alzheimer's disease in kindreds with missense mutations in a gene on chromosome 1 related to the Alzheimer's disease type 3 gene. Nature 376 (6543), 775–778. https://doi.org/10.1038/376775A0.

Romano, A., Pace, L., Tempesta, B., Lavecchia, A.M., Macheda, T., Bedse, G., Petrella, A., Cifani, C., Serviddio, G., Vendemiale, G., Gaetani, S., Cassano, T., 2014. Depressive-like behavior is paired to monoaminergic alteration in a murine model of Alzheimer's disease. Int. J. Neuropsychopharmacol. 18 (4), 1–12. https://doi.org/10.1093/IJNP/PYU020.

Rosell-Valle, C., Pedraza, C., Manuel, I., Moreno-Rodríguez, M., Rodríguez-Puertas, R., Castilla-Ortega, E., Caramés, J.M., Gómez Conde, Zambrana-Infantes, E., Ortega-Pinazo, J., Serrano-Castro, P.J., Chun, J., Rodríguez De Fonseca, F., Santín, L.J., Estivill-Torrús, G., 2021. Chronic central modulation of LPA/LPA receptors-signaling pathway in the mouse brain regulates cognition, emotion, and hippocampal neurogenesis. Prog. Neuropsychopharmacol. Biol. Psychiatry 108, 110156. https://doi.org/10.1016/j.pnpbp.2020.110156.

Ruegsegger, G.N., Creo, A.L., Cortes, T.M., Dasari, S., Nair, K.S., 2018. Altered mitochondrial function in insulin-deficient and insulin-resistant states. J. Clin. Investig. 128 (9), 3671–3681. https://doi.org/10.1172/JCI120843.

Sako, N., Shimura, T., Komure, M., Mochizuki, R., Matsuo, R., Yamamoto, T., 1994. Differences in taste responses to Polycose and common sugars in the rat as revealed by behavioral and electrophysiological studies. Physiol. Behav. 56 (4), 741–745. https://doi.org/10.1016/0031-9384(94)90236-4.

Sánchez-Alegría, K., Flores-León, M., Avila-Muñoz, E., Rodríguez-Corona, N., Arias, C., 2018. PI3K signaling in neurons: a central node for the control of multiple functions. Int. J. Mol. Sci. 19 (12) https://doi.org/10.3390/IJMS19123725.

Scheggi, S., De Montis, M.G., Gambarana, C., 2018. Making sense of rodent models of anhedonia. Int. J. Neuropsychopharmacol. 21 (11), 1049. https://doi.org/10.1093/IJNP/PYY083.

Schneider, C.A., Rasband, W.S., Eliceiri, K.W., 2012. NIH Image to ImageJ: 25 years of image analysis. Nature Methods 9 (7), 671–675. https://doi.org/10.1038/nmeth.2089. NIH Public Access.

Schneider, F., Baldauf, K., Wetzel, W., Reymann, K.G., 2014. Behavioral and EEG changes in male 5xFAD mice. Physiol. Behav. 135, 25–33. https://doi.org/10.1016/J.PHYSBEH.2014.05.041.

Schwartz, M.W., Woods, S.C., Porte, D., Seeley, R.J., Baskin, D.G., 2000. Central nervous system control of food intake. Nature 404 (6778), 661–671. https://doi.org/10.1038/35007534.

Segovia-Rodríguez, L., Echeverry-Alzate, V., Rincón-Pérez, I., Calleja-Conde, J., Bühler, K.M., Giné, E., Albert, J., Hinojosa, J.A., Huertas, E., Gómez-Gallego, F., Bressa, C., Rodríguez de Fonseca, F., López-Moreno, J.A., 2022. Gut microbiota and voluntary alcohol consumption. Transl. Psychiatry 12 (1). https://doi.org/10.1038/S41398-022-01920-2.

Serrano-Pozo, A., Frosch, M.P., Masliah, E., Hyman, B.T., 2011. Neuropathological alterations in Alzheimer disease. Cold Spring Harb. Perspect. Med. 1 (1) https://doi.org/10.1101/CSHPERSPECT.A006189.

Sherrington, R., Rogaev, E.I., Liang, Y., Rogaeva, E.A., Levesque, G., Ikeda, M., Chi, H., Lin, C., Li, G., Holman, K., Tsuda, T., Mar, L., Foncin, J.F., Bruni, A.C., Montesi, M.P., Sorbi, S., Rainero, I., Pinessi, L., Nee, L., St George-Hyslop, P.H., 1995. Cloning of a gene bearing missense mutations in early-onset familial Alzheimer's disease. Nature 375 (6534), 754–760. https://doi.org/10.1038/375754A0.

Shukla, P.K., Delotterie, D.F., Xiao, J., Pierre, J.F., Rao, R., McDonald, M.P., Khan, M.M., 2021. Alterations in the gut-microbial-inflammasome-brain axis in a mouse model of Alzheimer's disease. Cells 10 (4). https://doi.org/10.3390/CELLS10040779.

Steen, E., Terry, B.M., Rivera, E.J., Cannon, J.L., Neely, T.R., Tavares, R., Xu, X.J., Wands, J.R., De La Monte, S.M., 2005. Impaired insulin and insulin-like growth factor expression and signaling mechanisms in Alzheimer's disease – is this type 3 diabetes? J. Alzheimer's Dis. 7 (1), 63–80. https://doi.org/10.3233/JAD-2005-7107.

Strekalova, T., Spanagel, R., Bartsch, D., Henn, F.A., Gass, P., 2004. Stress-induced anhedonia in mice is associated with deficits in forced swimming and exploration.

Neuropsychopharmacology 29 (11), 2007–2017. https://doi.org/10.1038/sj.npp.1300532.

Talbot, K., Wang, H.Y., Kazi, H., Han, L.Y., Bakshi, K.P., Stucky, A., Fuino, R.L., Kawaguchi, K.R., Samoyedny, A.J., Wilson, R.S., Arvanitakis, Z., Schneider, J.A., Wolf, B.A., Bennett, D.A., Trojanowski, J.Q., Arnold, S.E., 2012. Demonstrated brain insulin resistance in Alzheimer's disease patients is associated with IGF-1 resistance, IRS-1 dysregulation, and cognitive decline. J. Clin. Invest. 122 (4), 1316–1338. https://doi.org/10.1172/JCI59903.

Tang, X., Wu, D., Gu, L.-H., Nie, B.-B., Qi, X.-Y., Wang, Y.-J., Wu, F.-F., Li, X.-L., Bai, F., Chen, X.-C., Xu, L., Ren, Q.-G., Zhang, Z.-J., Tang, X., Wu, D., Gu, L.-H., Nie, B.-B., Qi, X.-Y., Wang, Y.-J., Zhang, Z.-J., 2016. Spatial learning and memory impairments are associated with increased neuronal activity in 5XFAD mouse as measured by manganese-enhanced magnetic resonance imaging. Oncotarget 7 (36), 57556–57570. https://doi.org/10.18632/ONCOTARGET.11353.

Tanzi, R.E., Bertram, L., 2005. Twenty years of the Alzheimer's disease amyloid hypothesis: a genetic perspective. Cell 120 (4), 545–555. https://doi.org/10.1016/J.CELL.2005.02.008.

Tran, T.T.T., Corsini, S., Kellingray, L., Hegarty, C., Le Gall, G., Narbad, A., Uller, M.M., Tejera, N., O'toole, P.W., Minihane, A.-M., Vauzour, D., 2019. APOE genotype influences the gut microbiome structure and function in humans and mice: relevance for Alzheimer's disease pathophysiology. FASEB J. 33, 7. https://doi.org/10.1096/fj.201900071R.

Tzakis, N., Holahan, M.R., 2019. Social memory and the role of the hippocampal CA2 region. Front. Behav. Neurosci. 13, 233. https://doi.org/10.3389/FNBEH.2019.00233/BIBTEX.

Vogt, N.M., Kerby, R.L., Dill-McFarland, K.A., Harding, S.J., Merluzzi, A.P., Johnson, S.C., Carlsson, C.M., Asthana, S., Zetterberg, H., Blennow, K., Bendlin, B.B., Rey, F.E.,

2017. Gut microbiome alterations in Alzheimer's disease. Sci. Rep. 7 (1) https://doi.org/10.1038/S41598-017-13601-Y.

Wang, W., Tanokashira, D., Fukui, Y., Maruyama, M., Kuroiwa, C., Saito, T., Saido, T.C., Taguchi, A., 2019. Serine phosphorylation of IRS1 correlates with Aβ-unrelated memory deficits and elevation in Aβ level prior to the onset of memory decline in AD. Nutrients 11 (8), 1–18. https://doi.org/10.3390/nu11081942.

Xu, F., Na, L., Li, Y., Chen, L., 2020. RETRACTED ARTICLE: roles of the PI3K/AKT/mTOR signalling pathways in neurodegenerative diseases and tumours. Cell Biosci. 10 (1), 1–12. https://doi.org/10.1186/S13578-020-00416-0.

Yu, H.-J., Koh, S.-H., 2017. The role of PI3K/AKT pathway and its therapeutic possibility in Alzheimer's disease. Hanyang Med. Rev. 37 (1), 18. https://doi.org/10.7599/hmr.2017.37.1.18.

Zhang, Y., Huang, N. Qu, Yan, F., Jin, H., Zhou, S. Yu, Shi, J. Shan, Jin, F., 2018. Diabetes mellitus and Alzheimer's disease: GSK-3β as a potential link. Behav. Brain Res. 339, 57–65. https://doi.org/10.1016/J.BBR.2017.11.015.

Zhao, Y., Dua, P., Lukiw, W., 2015. Microbial sources of amyloid and relevance to amyloidogenesis and Alzheimer's disease (AD). J. Alzheimer's Dis. Parkinsonism 5 (1), 177. https://doi.org/10.4172/2161-0460.1000177.

Zheng, M., Wang, P., 2021. Role of insulin receptor substance-1 modulating PI3K/Akt insulin signaling pathway in Alzheimer's disease. *3*. Biotech 11 (4), 1–17. https://doi.org/10.1007/s13205-021-02738-3.

Zhuang, Z.Q., Shen, L.L., Li, W.W., Fu, X., Zeng, F., Gui, L., Lü, Y., Cai, M., Zhu, C., Tan, Y.L., Zheng, P., Li, H.Y., Zhu, J., Zhou, H.D., Le Bu, X., Wang, Y.J., 2018. Gut microbiota is altered in patients with Alzheimer's disease. J. Alzheimers Dis. 63 (4), 1337–1346. https://doi.org/10.3233/JAD-180176.